Developing Mining Camp Exploration Concepts and Technologies – Brownfield Exploration Project 2013–2016
Edited by Soile Aatos
Geological Survey of Finland, Special Paper 59, 113–138, 2016

GEOPHYSICAL SURVEYS OF THE MIIHKALI AREA, EASTERN FINLAND

by

Ilkka Lahti[1)], Hanna Leväniemi[2)], Asko Kontinen[3)], Peter Sorjonen-Ward[3)], Soile Aatos[3)] and Esko Koistinen[3)]

Lahti, I., Leväniemi, H., Kontinen, A., Sorjonen-Ward, P., Aatos, S. & Koistinen, E. 2016. Geophysical surveys of the Miihkali area, Eastern Finland. *Geological Survey of Finland, Special Paper 59*, 113–138, 26 figures and 1 table.

The Miihkali area in the northeastern Outokumpu ore belt is an excellent place to carry out geophysical research, as the area is characterized by diverse geophysical anomalies and is also prospective for Outokumpu-type massive sulphide ore deposits. In this paper, we deal with geophysical surveys that have been conducted during the last decades in the area, including ground electromagnetic (EM) and potential field surveys, airborne surveys and petrophysical measurements of drill cores. These data have been acquired by the Outokumpu Mining Company, the Geological Survey of Finland, and their joint venture, the GEOMEX project. We also report new data from deep EM (ZTEM and AMT) surveys carried out during the ongoing Outokumpu (OKU) mining camp project. All these geophysical data are summarized and modelled from various standpoints, and the geological implications are discussed.

The potential field datasets predate the current project. In this study, we tested both 3D forward modelling and inversion as deep exploration tools. The results imply that the current drilling scope covers the majority of the anomaly sources, although some discrepancies remain between the new density model and the drill core logs. We applied 3D inversion to a regional magnetic dataset with partial success; it became clear that comprehensive interpretation would need to accommodate for remanent magnetization, which plays a significant role in magnetic modelling in the Miihkali region. The 3D models suggest that the deep-set magnetic and high-density features east of the more shallow main Miihkali massif may not be thoroughly explored, and further work on these features could provide some previously undiscovered information on the Miihkali massif region.

Deep EM results show conductors along the western margin of the Miihkali mica gneisses and the Miihkali serpentinite massif. The ZTEM and AMT 2D inversion results indicate a gently eastwards-dipping conductor in the Miihkali mica gneiss located at the bottom of the inferred Miihkali nappe, reaching depths greater than 1 km near to its eastern margin. The gently dipping conductor is probably related to the N–S elongated airborne EM anomalies coinciding with the Miihkali serpentinite massif and the black schist band along the western margin of the allochthonous Miihkali mica gneisses. In most cases, the near-surface airborne EM anomalies can be

connected to deep ZTEM anomalies, showing the continuation of elongated conductive features to greater depths. The densely spaced Sampo soundings distinguished separate conductors in the Miihkali serpentinite massif and within the western margin of the Miihkali mica gneisses. In addition, the Sampo surveys revealed conductors at the Kiskonjoki prospect, which have been proved to be caused by Outokumpu-type rocks intersected by drillings at the depth of 300 m.

Keywords: geophysical surveys, geophysical methods, gravity method, magnetic method, electromagnetic methods, airborne methods, Outokumpu area

[1)] *Geological Survey of Finland, P.O. Box 77, FI-96101 Rovaniemi, Finland*
[2)] *Geological Survey of Finland, P.O. Box 96, FI-02151 Espoo, Finland*
[3)] *Geological Survey of Finland, P.O. Box 1237, FI-70211 Kuopio, Finland*

E-mail: ilkka.lahti@gtk.fi

GEOLOGICAL SETTING

The Miihkali area is located within the northern part of the largely metasedimentary early Proterozoic North Karelia Schist Belt (NKSB) (Fig. 1). The main content of the c 12 000 km² NSKB are Kaleva stage (2.1–1.9 Ga) intercalated wackes and shales. Older, Sariola (2.3–2.2 Ga) and Jatuli stage (2.2–2.1 Ga) arenitic sequences are found narrowly rimming the belt in the north and east, deposited on a deeply eroded dominantly gneissic-migmatitic granitoid (>2.6 Ga) basement. A major part of the main Kaleva fill is composed of deep-water metaturbidites that contain zones of black schists, the latter in part with sheets and lenses of serpentinized peridotites±metagabbroic–amphibolitic rocks interpreted as fault-bound ophiolite fragments. The ophiolite-bearing parts of the NSKB have long been considered allochthonous (Wegmann 1928, 1929, Väyrynen 1939, Koistinen 1981, Park & Bowes 1983, Park & Doody 1990), and are collectively known as the Outokumpu nappe/nappe complex or allochthon (Park & Doody 1990, Peltonen et al. 2008). The Saramäki sulphide deposit (Hallikainen 1980) is located in the present study area.

A special feature of the Outokumpu allochthon is that the peridotite bodies in the included ophiolite fragments are all not only serpentinized but also thinly altered (max 50 m) at their margins to carbonate, carbonate-silica and silica rocks (birbirites). This alteration occurred before or early during the regional deformation and metamorphism (Kontinen 1998, Peltonen et al. 2008). The alteration appears to have been most intense where the parent serpentinized peridotite bodies were/are located against particularly thick layers of sulphide-graphite rich black shale. The assemblage of serpentinite-carbonate-calc-silicate rock-quartz rock-black schist constitute the Outokumpu association or assemblage (Gaal et al. 1975, Park 1988), famous for being the host environment of the Outokumpu-type massive-semi-massive

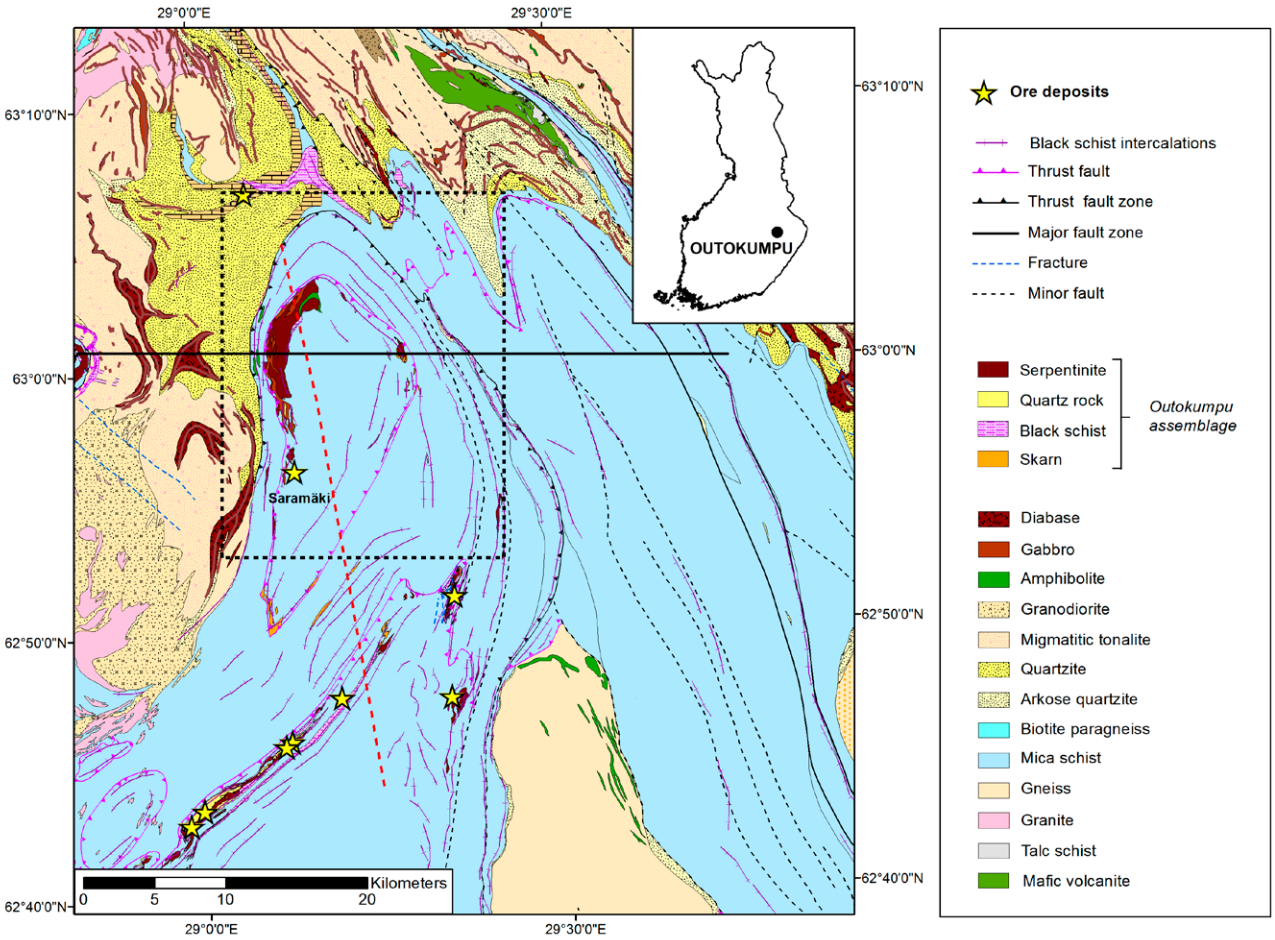

Fig. 1. Geological map of the study area (Bedrock of Finland – DigiKP). The dashed rectangle indicates the location of the study area. The location of the cross-section view in Figure 2 is shown by the black E–W line (N=6990000). The red dashed line denotes the approximate location of the antigorite-out isograd from Säntti et al. (2006), implying <550 °C peak-M conditions to the east and >550 °C to the west of the line.

Co-Cu-Zn sulphide ores (Gaal & Parkkinen 1993, Peltonen et al. 2008).

The Miihkali area comprises the northernmost part of the eastern main segment of the Outokumpu allochthon. The allochthon rests in the area on an Archaean-aged, dominantly granite gneissic basement thinly covered by a relatively flat-lying Early Proterozoic (Jatuli-stage) sequence of cratonic-epicontinental feldspathic to quartz arenitic metasands with some thin calc silicate rock–carbonaceous metapelite intercalations. The interface of the basement and the Jatuli sequence is intruded by laterally extensive, up to 200-300 m thick, metamorphosed-deformed pyroxenite-gabbro-leucogabbro sills. The basal contact of the allochthon is defined in the area by a thrust fault with thin slivers of obvious Archaean gneisses, as seen, for example, at Saarivaara and Matovaara, west of Lake Miihkalinjärvi.

In the study area, the Outokumpu allochthon is traditionally divided, largely based on the interpretation of anomaly patterns on geophysical maps, into two overlapping thrust sheets or nappes (e.g. Park & Doody 1990, Sorjonen-Ward et al. 1997). The lower one, in the area of the basal unit of the Outokumpu allochthon, we refer to as the Sukkulansalo nappe, while we refer to the discontinuously serpentinite and black schist-rimmed, c. 10 x 25 km oval feature in the middle part of the Miihkali area as the Miihkali nappe. This is traditionally interpreted as a down-folded thrust sheet into a structural basin on the Sukkulansalo nappe.

There are a few minor lenses of ophiolitic rocks in the Sukkulansalo nappe, whereas the interpreted western basal part of the Miihkali nappe hosts perhaps the largest cohesive serpentinite-mafic massif so far recognized in the Outokumpu allochthon, the near 15 km long and up to 1.5 km wide Miihkali massif. Unlike the better known bodies in the Outokumpu-Vuonos-Horsmanaho zone, which tend to be >90% ultramafic, there is a variably significant, in some parts over 50% mafic, mostly coarse-grained, foliated metagabbroic component within the Miihkali massif. Most of this component occurs as relatively thin dykes or sills in the serpentinite; for example, within a 735 m, near perpendicular section through the massif, the drill hole Jumi-46 contains 38.4% (n = 79) mafic sheets/dykes averaging 3.58 ± 6.54 m in thickness. This may be exploration-wise an important aspect to recognize, as the Outokumpu alteration assemblage appears to be a noticeably less abundant component in the Miihkali massif than in the sulphide-ore-blessed Outokumpu, Vuonos or Kylylahti massifs (Saastamoinen 1972). It must be noted here that the drill-core logging by the Outokumpu company for the Miihkali prospect was predominantly rather sketchy, failing to consistently distinguish skarns (calc-silicate rocks) from metabasic rocks (metagabbros and amphibolites) and ultramafic-derived quartz rocks (metabirbirites) from epiclastic quartzites, and lumping together the various, petrophysically differing types of ultramafic rocks (antigorite serpentinite, serpentinized talc-olivine and olivine-talc-carbonate rock). The ambiguity in rock identification and naming severely complicates and reduces the usability of the drilling-related lithology database.

An important factor to consider in most geophysical interpretations is the increasing metamorphic grade from east to west in the Miihkali area. A change from lower to middle amphibolite facies takes place across a line running approximately N–S through the middle of the Miihkali area, coinciding with the antigorite out/talc-olivine (in low CO_2/H_2O) reaction in ultramafic rocks (Säntti et al. 2006). The discordant nature of the isograd implies that the peak metamorphism post-dated the main deformations. Because of the metamorphic zoning, ultramafic bodies in the eastern part of the area are antigorite serpentinites grading towards their margins (towards higher CO_2/H_2O at the peak of metamorphism) to carbonate-antigorite serpentinites and talc-carbonate rocks, whereas in the western part these rocks are transformed into talc-olivine rocks and distinctly olivine porphyroblastic (”dalmatian”) talc-carbonate rocks. In a similar way, only tremolite is met in calc-silicate rocks in the east, whereas diopside appears in compositionally similar rocks in the west. The reactions involved increase rock density (Lehtonen 1981, Leväniemi 2016 (this volume)), and also contribute to the rock magnetic properties, but these effects are complicated by the usually extensive retrogression of ferromanganese minerals, especially olivine, to lizardite and chrysotile serpentine.

No detailed field-based study has yet been carried out on the structural geology of the Miihkali area. All existing structural interpretations have been presented in connection with broader regional overviews, based on rock distribution and structural data on 1:100 000 scale maps, which were compiled during the 1970s (based on data mainly collected by trainee students), and on the interpretation of geophysical anomaly maps. Some

attempts to geophysically evaluate/model the Miihkali structure were made by the Outokumpu company, but the results were mostly only presented in company reports (e.g. Ketola 1973, Ketola 1974, Soininen 1979, Lehtonen 1980). An early attempt to model the 3D structure of the whole northern part of the eastern NKSB is included in an exploration report by Saastamoinen (1972), in the form of a block diagram constructed on seven interpreted SW–NE trending cross-sections. The diagram was prepared before the major revitalization of the early adopted Alpine concepts in the 1980s (Wegmann 1928, Väyrynen 1939) in the analysis of the tectonic nature of the NKSB, but now from a plate tectonic perspective (e.g. Koistinen 1981, Park & Bowes 1983, Park et al. 1984, Park & Doody 1990). Reflecting its time of completion, the interpretation in Saastamoinen (1972) makes no distinction between autochthonous and allochthonous units, and the Kalevian deep water sedimentary rocks are also considered autochthonous materials sedimented in a geosynclinal basin and the enclosed serpentinites as intrusive units. For the geosynclinal Kaleva, a maximum thickness of about 5 km was inferred in the middle part of the Miihkali area. The Kalevian sediments were seen as directly deposited on the Archaean basement or its thin cover of Jatulian quartzites.

In the more recent regional structural models (e.g. Koistinen 1981, Park & Bowes 1983, Park et al. 1984, Sorjonen-Ward et al. 1997), the Miihkali nappe is usually interpreted as an erosional remnant of the Outokumpu nappe that now includes as its main preserved part the Viinijärvi "basin" delineated in the west by the Outokumpu–Vuonos–Horsmanaho and in the east by the Sola–Onkilahti–Petäjäjärvi serpentinite black schist chains. As there is a quite distinct difference in the mafic-ultramafic ratio between the Miihkali and Outokumpu ophiolite fragments, it is possible that they represent different oceanic proto-sources, and hence their Miihkali and Outokumpu hosts possibly separate nappe sheets. We note here that in their synthesis across the NKSB, Park and Doody (1990, Fig. 11) correlated the Miihkali structure with their Kaavi area "duplexes". Large recumbent folds have been interpreted as an early (F1) character of the Viinijärvi basin or synform (Koistinen 1981, Park & Doody 1990). If the routinely assumed direct correlation of Miihkali and Viinijärvi was true, the possibility of early recumbent folds should also be assumed in the Miihkali nappe.

Finally, we note that the customary interpretation of the Sukkulansalo and Miihkali nappes forming a simple synformal structural basin is in fact in conflict with structural data on the published geological maps, which show that across the entire central part of the assumed basin, schistosities systematically dip eastwards (<20–60 degrees) and do not therefore define any structural basin. Our own observations for c. 50 outcrops across the central part of the Miihkali nappe are in agreement, as in all of these outcrops, an east-dipping spaced foliation was the most readily observable structural aspect. Even more critically, we found from this tentative mapping that bedding was

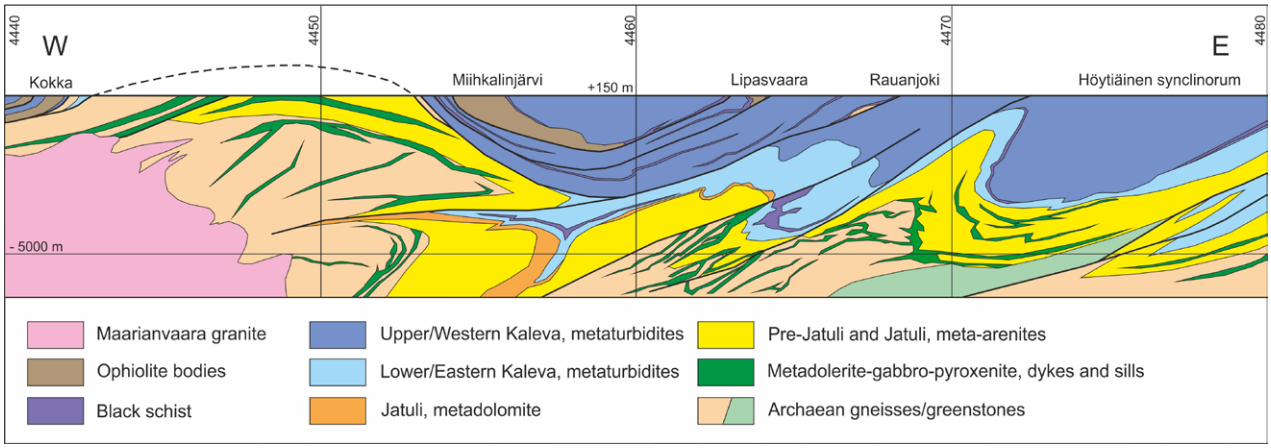

Fig. 2. Interpreted geological cross-section (E–W along the KKJ4 northing line N=6990000) of the Miihkali area. The surface of the section sketch is based on published geological maps and deeper parts on simple down-plunge extrapolation from the northern contact of the NKSB, located 5–10 km north of the section line. Although its details are certainly inaccurate, the sketch should nevertheless provide a reasonable idea of the general structural style, at least regarding the deformation of the basement–cover interface. The inferred basal faults of the Sukkulansalo (at Rauanjoki) and Miihkali nappe sheets (at Lipasvaara) are marked, but no attempt is made to illustrate the currently poorly known structural patterns inside the nappe sheets or Höytiäinen synclinorum.

also mostly dipping to the east, although gently N or S plunging outcrop-scale S-type folds were locally observed to cause minor complications to this simple general pattern. Importantly, we also saw no outcrop evidence suggestive of the expected (see above) isoclinal/recumbent F1 folding. One option is that the Miihkali basin was actually defined by a west overturned asymmetrical syncline (with a steeper eastern limb), although this model also requires subsequent faulting to explain departures from the expected ideal structural (foliation/So) pattern.

If the Miihkali nappe is still poorly understood, even less is known for certain about the internal structure of the underlying Sukkulansalo nappe. Overall, the only reconnaissance-style general mapping currently available for the area does not allow a truly meaningful structural analysis, which we assess would be a very difficult task, even if detailed, structurally-oriented field mapping was carried out, given the missing topographical relief and only mediocre exposure in the area. Quite plentiful and partly fairly deep-reaching (up to 1.2 km) drilling helps to constrain the structure of the western part of the Miihkali area, but in the eastern part there are only a few deeper holes concentrated around the Lipasvaara talc-mining site. Figure 2 presents an interpreted geological cross-section (E–W) of the area.

POTENTIAL FIELD MODELLING

The potential field dataset for the region modelled in this study (Fig. 3a) comprises systematic line-based and regional gravity data collected by Outokumpu Oy (Ketola 1973) and the airborne magnetic dataset of GTK (Hautaniemi et al. 2005).

The systematic gravity survey comprises Bouguer anomaly data with mainly 100 and 200 m line spacing and 20 m sample spacing along the lines. The station density for the regional gravity data in the study area is 4.65 p/km^2 in the west and c. 2 p/km^2 in the east (Fig. 3c). The modelling dataset was constructed by combining the interpolated grids of the systematic and regional surveys so that the former data (first corrected for level) were used where available and the latter were used to fill the remaining regions (Fig. 3d). The final modelling dataset was sampled from the combined grid with 500 m line spacing and 50 m sample spacing along lines that cross the study area in an east–west direction.

The magnetic dataset (Fig. 3b) contains data from the Juankoski airborne survey area completed in August-September 1980, corresponding to an IGRF total field intensity of 52 129 nT, field inclination 74.5° and declination 7.5°. The survey was conducted with 200 m line spacing; in the study area, the median sample spacing was 24 m and the median altitude 35 m. For this work, the data were interpolated with 50 m cell spacing, upward continued to 50 m altitude for noise-reduction purposes and finally sampled with 100 m line spacing (east–west lines) and 50 m sample spacing. The regional level of 51 300 nT was removed from the data.

We used both forward modelling and 3D inversion in interpreting the Miihkali potential field dataset. The density model was constructed using forward modelling. This approach was selected due to the abundance of drill hole data that could be used in model construction and also because of the double-peaked density distribution of the Miihkali massif rocks (see Leväniemi 2016), which proved challenging for the inversion algorithms tested in the course of the work. The aeromagnetic data for the Miihkali region were modelled with 3D inversion algorithms. We employed the UBC-GIF inversion algorithm MAG3D v4.0 (e.g. Li & Oldenburg 1996) run via the Pitney Bowes ModelVision v14.0 interface; the latter was also used for all forward modelling.

Gravity modelling

The forward modelling was performed on east–west-trending lines with 500 m line spacing and 50 m station spacing. Terrain topography was included in the model. The Bouguer anomaly map (Fig. 3d) shows two main gravity components: a broad, long-wavelength regional maximum and more local features, most of which are probably related to the Miihkali massif. The modelling was respectively performed in two phases: firstly, the generation of the regional level model, and then modelling of the ultramafic massif.

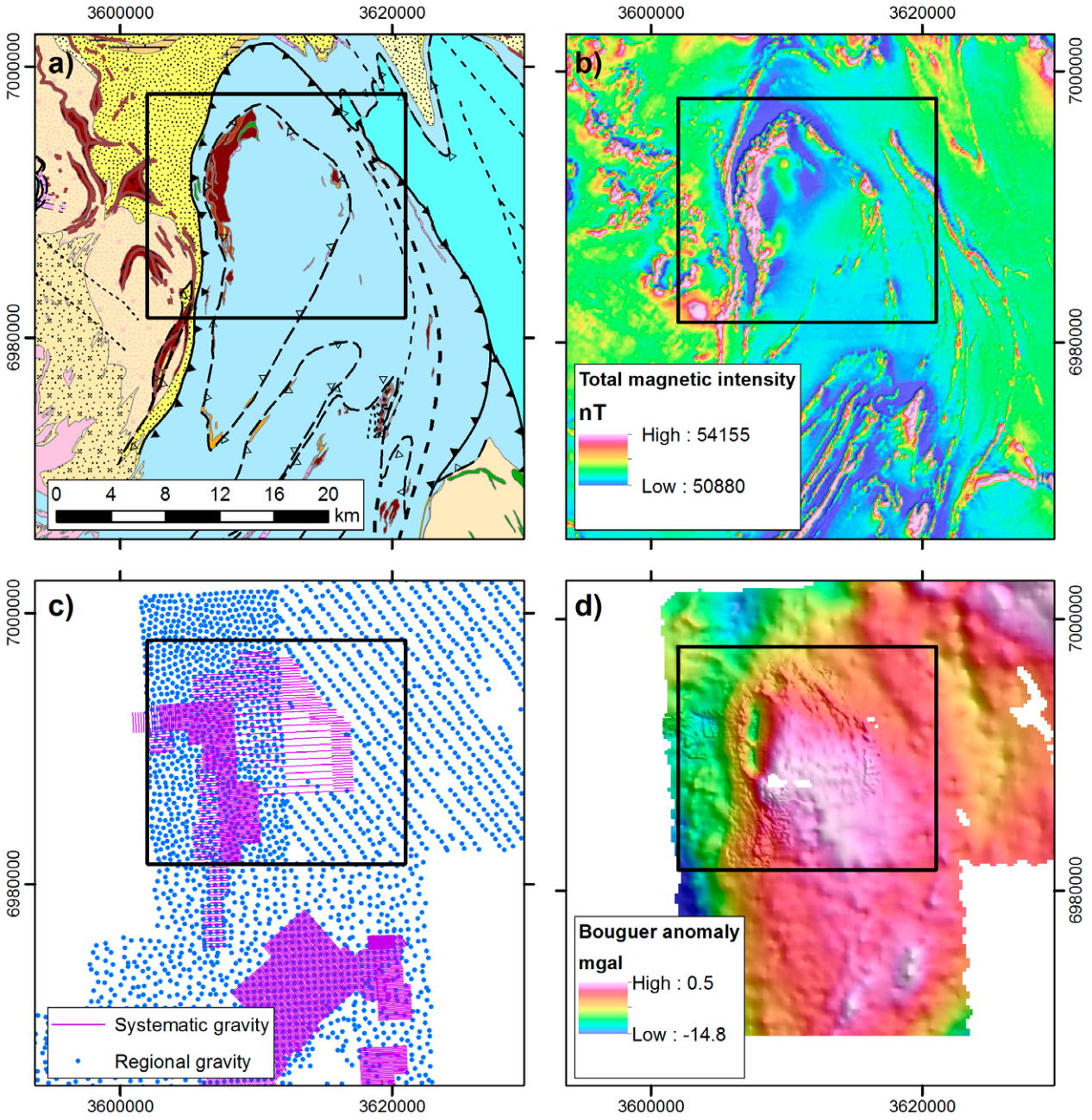

Fig 3. a) Geological map of the area (potential field modelling region outlined in black) (Bedrock of Finland – DigiKP), b) an aeromagnetic map, c) gravity data sampling locations for systematic and regional datasets, and d) a Bouguer anomaly of the gravimetric dataset.

Regional level

A wide long-wavelength anomaly located in the mid-part of the study area (Fig. 3d) is assumed to be caused by the metasediments ('mica schists') that lie over the slightly lower-density Archaean basement, as earlier demonstrated by Ketola (1974). In the model, the mica schist density was set to a relative value of 0.08 g/cm^3 (in comparison to the Archaean gneisses) (see Leväniemi 2016) and the model regional level at -8.5 mgal. With these parameters, we were able to model the mica schists with a 3D model body that has a maximum thickness of less than 3 km and a western contact dipping towards the east (Fig. 4).

The regional level model conforms moderately well to the geological cross-section presented in geology chapter (Fig. 2) and in Figure 5, and as such it is plausible that the regional gravity maximum is mainly caused by the metasediments. Any mafic dykes and sills within the underlying Jatuli and Archaean rock are assumed to be of

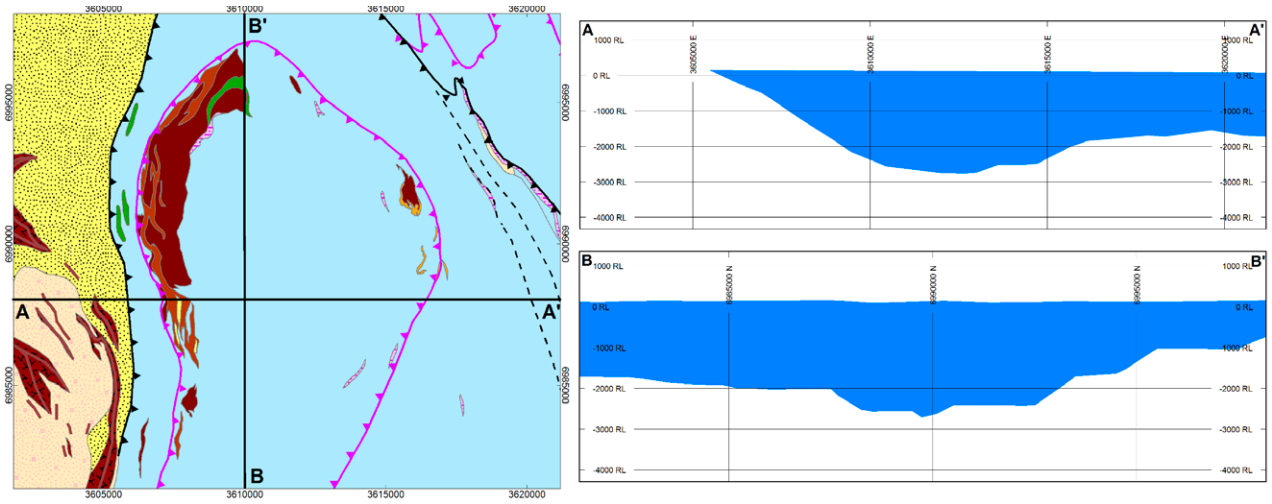

Fig. 4. Two cross-sections of the regional level model.

relatively high density and would also contribute to the total anomaly, but with the currently available information, the undisputed separation of various regional anomaly sources is unavoidably infeasible.

The calculated gravity response of the mica schist model body was removed from the original Bouguer anomaly data in order to disclose the residual response, mainly comprising the response from the Miihkali massif rocks (Fig. 6).

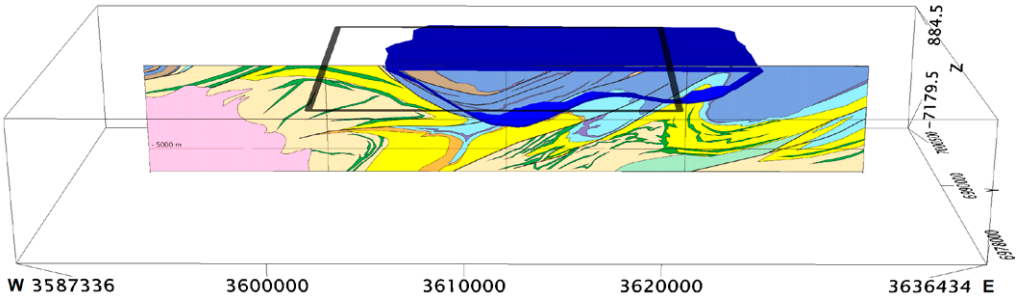

Fig. 5. Regional level model (dark blue) in comparison with the geological cross-section of N=6990000 (Fig. 2). The potential field modelling study area is outlined in black.

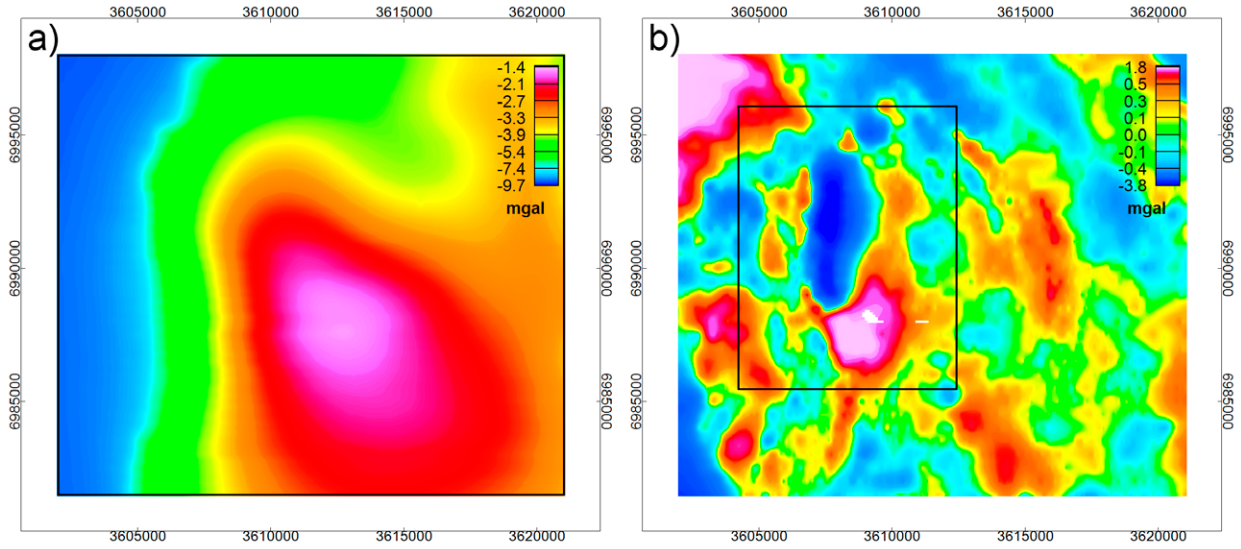

Fig. 6 a) Modelled response of the mica schist body, i.e. regional level and b) the gravity residual. Note the difference in the colour palettes. The residual data were only modelled for the region outlined in black on the gravity residual map.

Modelling of the Miihkali Massif

The residual gravity data for the Miihkali massif (Fig. 6) consist of gravity maxima and a distinct gravity minimum. This indicates that the massif is, in terms of densities, divided into a low-density part, i.e. the chrysotile serpentinite, and a high-density part, which comprises the rest of the Outokumpu altered ultramafic rocks (OAUM), as well as the metagabbros.

For the residual model, we used relative density values of −0.25 g/cm³ for the serpentinites and 0.18 g/cm³ for the OAUM rocks and metagabbros (in comparison to the mica schist; Leväniemi 2016). For the serpentinites, the density used in modelling was lower than the local median value of serpentinites (see Leväniemi 2016); this value was selected by comparing the modelling results with drilling: a lower density gives better-suited bottom depths for model bodies. We suggest this is because the modelled units contain few 'impurities' that would increase the density, i.e. the modelled units represent the low-value end of the density histogram, perhaps partly due to incompatibilities between the geological logging terminology and geophysical characteristics.

The final model is presented in Figure 7 and its response in comparison to the residual gravity data in Figure 8.

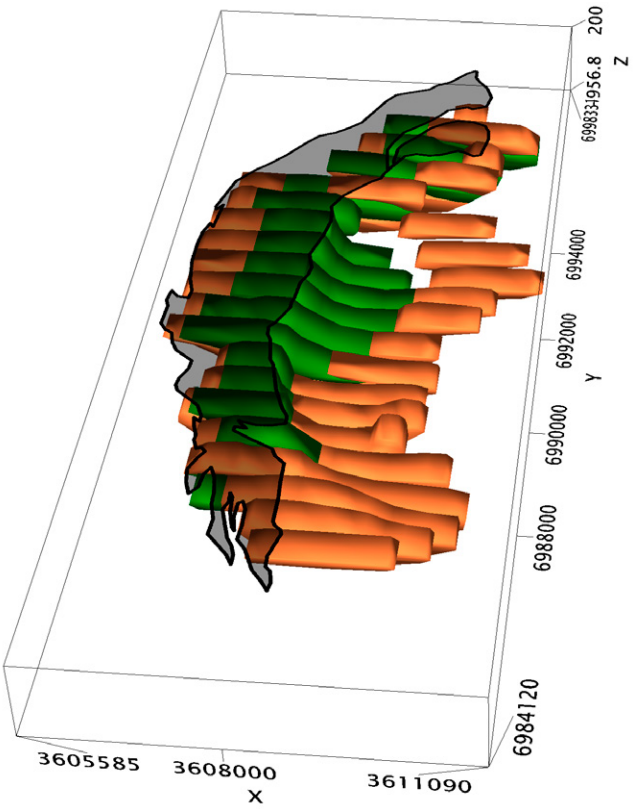

Fig. 7. The Miihkali massif density model, with the transparent gray surface part outlining the extent of the massif on the bedrock map. Model colours: Green = serpentinite, orange = OAUM rocks and metagabbros.

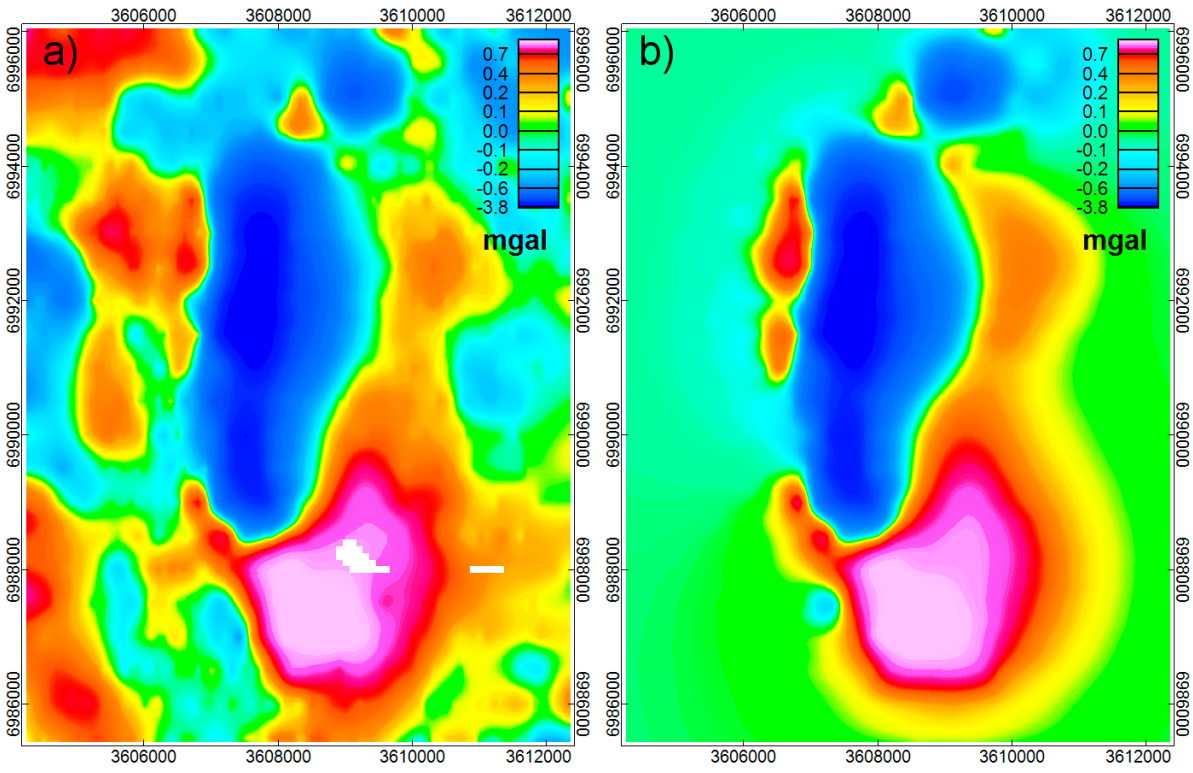

Fig. 8 a) The residual gravity data from Figure 6b, and b) the response from the model presented in Figure 7.

In the course of forward modelling, the classification data of the drill core lithology were used as guide in constructing the model bodies. However, as the model only uses two density values, some discrepancies between the drilling results and the model remain. For example, in Figure 9, in the eastern bottom part of the massif (e.g. drillhole JU-MI-114), black schists appear among the OAUM rocks, which lowers the bulk density; the model density may be assumed to be too high and consequently the bottom depth too shallow. In this profile, a noteworthy feature is the high-density feature at the eastern end of the massif; this was modelled as a curved, upward-reaching extension of the ultramafic rock.

In some cases, in order to maintain the best compatibility with drilling results, the low-density serpentinite sections in the drill hole were omitted, i.e. were assumed to be of high density. An example of this is shown in Figure 10.

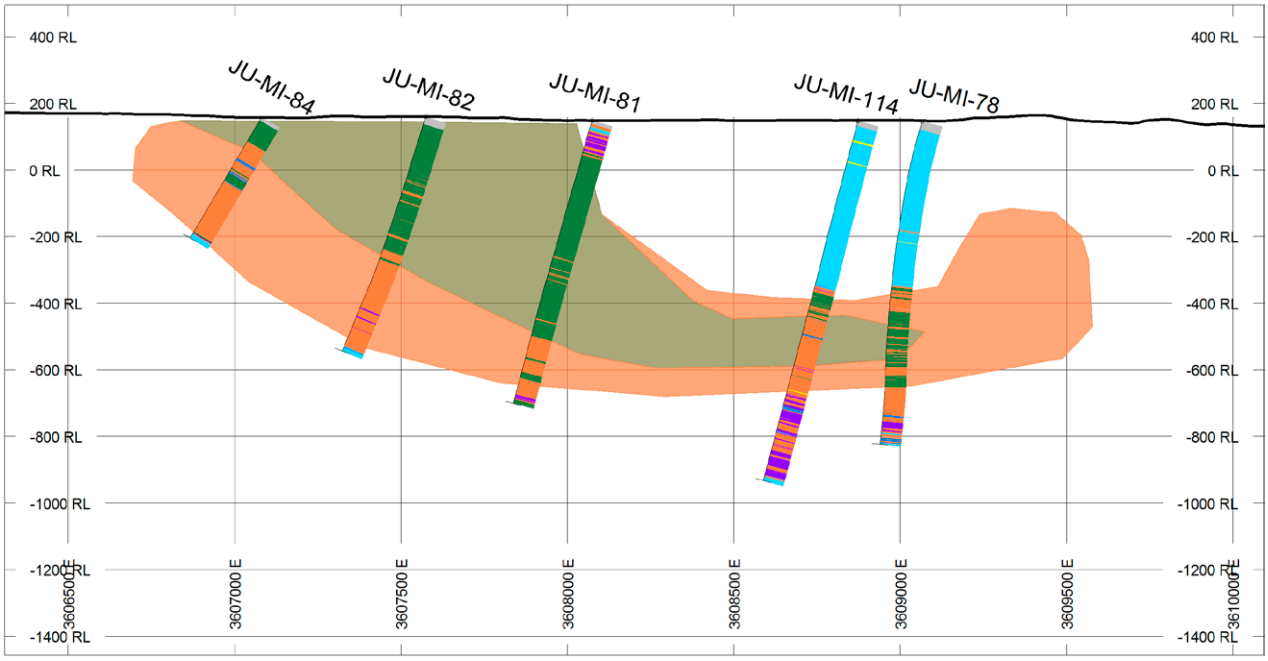

Fig. 9. Comparison of the gravity model with drill hole profile N=6989000 (Finland Uniform Coordinate System). Green = serpentinite, orange = OAUM rocks and metagabbros, purple = black schists, blue = mica schists.

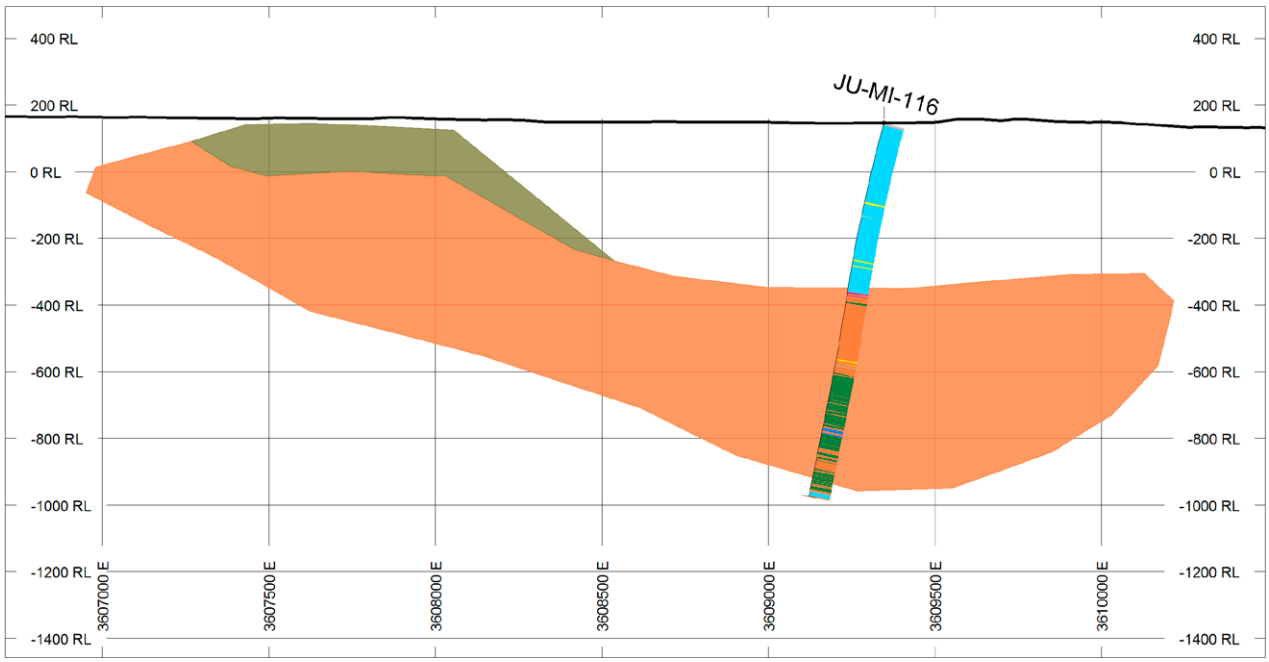

Fig. 10. Comparison of the gravity model with drill hole profile N=6988500. Green = serpentinite, orange = OAUM rocks and metagabbros, purple = black schists, blue = mica schists.

Modelling of the Saramäki deposit

The Saramäki mineralization south of the main massif (see Fig. 1) consists of a <20 m thick and 300 m wide sheet of dominantly disseminated to massive sulphides located in a relatively thin (<50–100 m) fault-bounded sliver of Outokumpu association rocks, mainly calc-silicate±carbonate rich skarns, but also skarnoid (Ca-metasomatised and metamorphosed) metabasic rocks (Kontinen et al. 2006). The sliver of Outokumpu-type rocks is enclosed in highly tectonized, mylonitic black and mica schists, apparently controlled by a NE striking, 20–25 degrees SW dipping fault plane. The main metals in the mineralization are, as is typical in OKU-type deposits, Co (0.086 wt%), Cu (0.71 wt%), Zn (0.63 wt%) and Ni (0.05 wt%) (Kontinen et al. 2006), although the grades are significantly lower than, for instance, in Outokumpu and Vuonos deposits. The ore has a moraine-covered surface exposure, from which it plunges, along with the sliver of OKU rocks, towards the northeast to the depth of at least 700 m. The metal grades increase towards greater depths. (Hallikainen 1980).

On the residual gravity anomaly map, presented with the regional (upward continued for 1 km) level removed, especially the region in the vicinity of the disseminated, low-grade ore outcrop appears as a local maximum (Fig. 11a). The magnetic vertical component data (Fig. 11b) show some of the deeper extension of the ore-hosting rock assemblage as a long-wavelength anomaly extending northeast from the sharp short-wavelength main anomaly zone resulting from shallow magnetic sources.

Two cross-sections of the mineralized zone (Fig. 12) highlight the petrophysical properties of the Saramäki deposit. On the southern section, at shallow depths (Fig. 12a), the highest drill core sample densities are mainly due to skarns and quartz rocks, except for a thin mineralization intersection in drill hole JU-MI-36. At the northern cross-section (Fig. 12b), the higher ore grades result in high densities; the relative proportion of skarns and carbonate rocks is lower at shallow depths in this cross-section. The highest magnetic susceptibilities correspond to skarns and black schists, but as discussed above, the remanent magnetization may greatly affect the magnetic anomaly signatures in this region.

To test the extent to which the measured gravity data can be explained with current knowledge of the Saramäki deposit, the data were inverted with the help of constraints based on the drill hole data (for drill-hole locations, see Figure 11b and c) using the UBC GRAV3D algorithm (Li & Oldenburg 1998). The mineralization is mainly hosted by skarn and skarnoid mafic rocks, the density of which is higher than that of the mica schist (Fig. 12), and the sequence can be followed from one drilling section to another (Fig. 13). A "high-density body" was built to surround this sheet-like host rock sequence (Fig. 14). In inversion, the density was required to

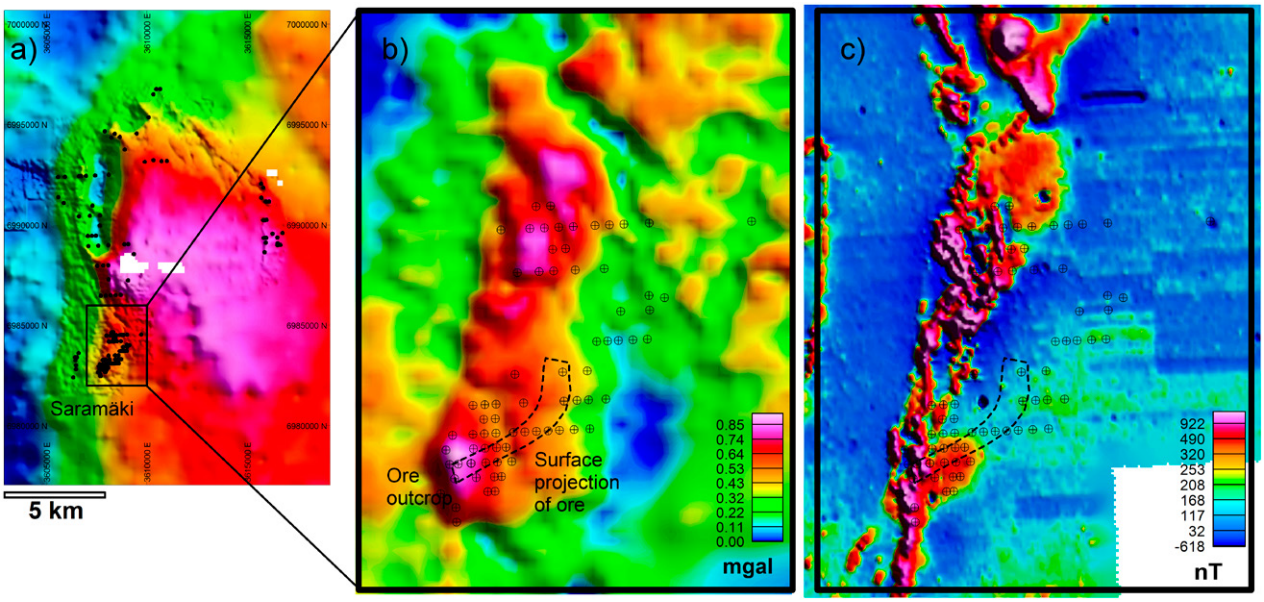

Fig. 11. The Saramäki deposit location on a) regional residual Bouguer anomaly map, b) detailed residual Bouguer anomaly map and c) magnetic vertical component map. Point symbols denote drill hole collar locations. Ore location and surface projection from Hallikainen 1980.

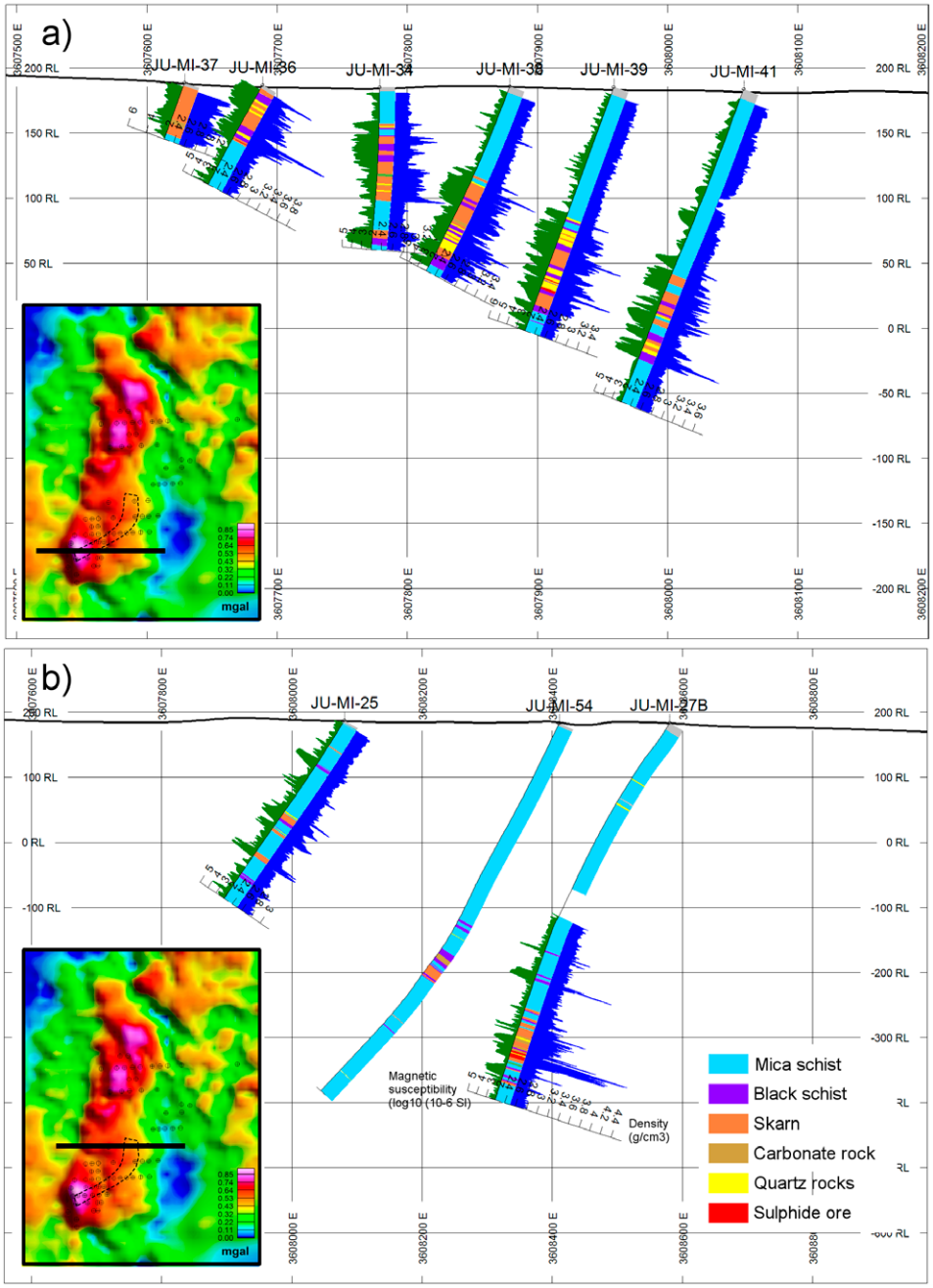

Fig. 12. Two E–W sections of the Saramäki deposit.

exceed a relative value of 0.1 g/cm^3 within this body; outside the body boundaries, the density was allowed to vary between -0.1 and 0.5 g/cm^3. The aim of inversion is to determine whether the recovered model suggests high densities outside the limiting body. The cell size in inversion is 50 by 50 m.

The resulting constrained inversion model (Fig. 15) suggests that either the high densities related to mineralization and its host rock do not extend further north than is covered by the current drilling, or, if there is continuation, the density contrast is not high enough to give rise to gravity anomalies in ground surveys. At the northern end of the model, the altered rocks of ultramafic origin in the Miihkali massif explain well the shallow density structures in the recovered inversion model.

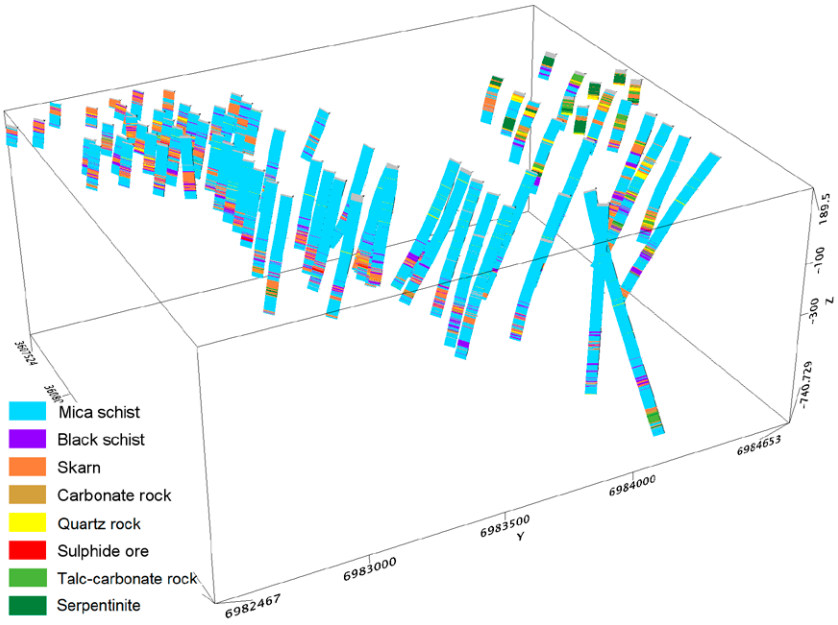

Fig. 13. Drill-hole lithologies.

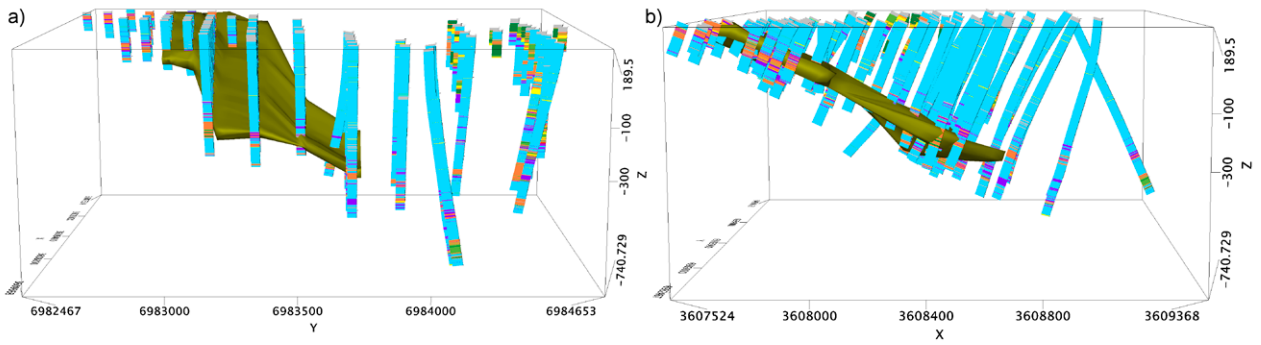

Fig. 14. The constraining high-density body viewed from the a) east and b) south.

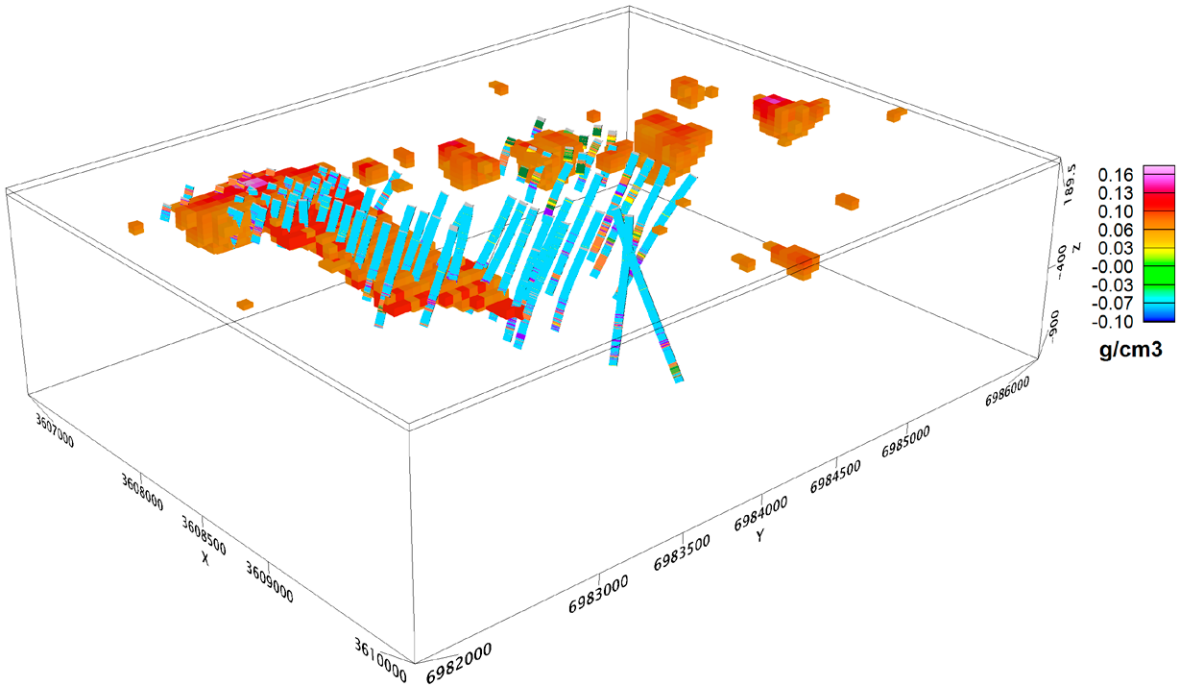

Fig. 15. The Saramäki 3D gravity inversion model (clipped at 0.06 g/cm^3).

Magnetic modelling

Magnetic modelling was conducted with the MAG3D inversion algorithm. The size of the study area was 19.0 km by 16.5 km; the inversion cell size in a horizontal direction was selected to be 100 m. The input data were upward-continued to a nominal altitude of 50 m prior to inversion. The inversion parameter values are listed in Table 1.

Remanent magnetization in inversion

In the Miihkali region, as in the Outokumpu region in general, there is one inversion precondition that is known not to be fulfilled: the inversion algorithms do not usually take remanent magnetization into account. However, most notably, the black schists in the study region are known to have high ratios of remanent to induced magnetization (Koenigsberger ratio or Q ratio). In Miihkali, the ratio for black schists is c. Q = 10 and the direction of remanent magnetization also deviates from the inducing field direction (inclination = 45°, declination = 90°) (Ahokas 1980), i.e. the magnitude of the remanent magnetization is ten-fold greater than the induced magnetization, and the magnetization direction also differs from that of the induced magnetization. For serpentinites and skarn rocks, Ahokas (1980) reports such wide value ranges and standard deviations that the generalized remanent magnetization parameters for these rocks cannot be established from the sample set.

Figure 16 presents a synthetic model response of a dipping black schist body 1) with induced magnetization only and 2) with added remanent magnetization, such as the body would appear in the Miihkali region. With remanent magnetization of this direction and magnitude, the amplitude of the modelled response is c. ten-fold greater in comparison to the response from the induced magnetization only; the shape of the anomaly is also notably different.

To examine the effect of remanent magnetization in inversion that only assumes induced magnetization to be present, unconstrained inversions of the calculated responses from the synthetic

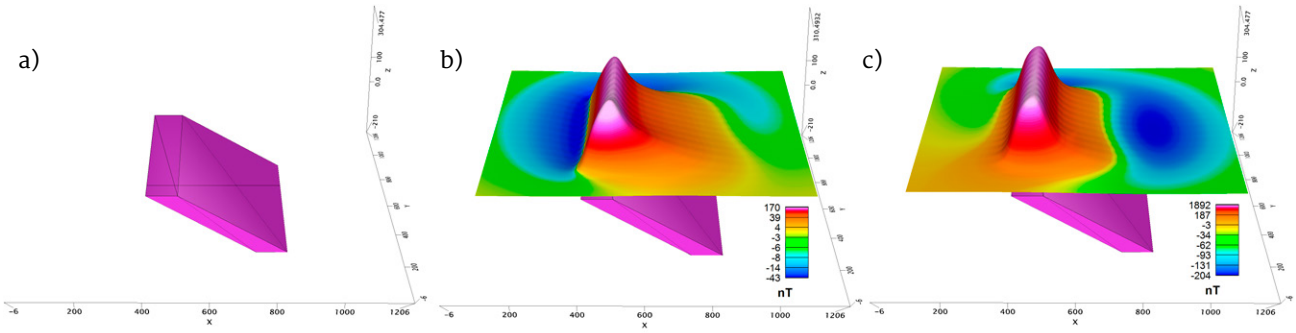

Fig. 16. a) Model body with dimensions 100 x 400 x 620 m and 30-degree dip, magnetic susceptibility k = 0.02 SI and the top surface at the depth of 10 m, the magnetic anomaly response b) without and (c) with remanent magnetization (Q = 10, I = 45° and D = 90°). The results are modelled at 15 m altitude with field parameters matching the Miihkali airborne survey. Note the difference in the magnitudes of the magnetic anomalies.

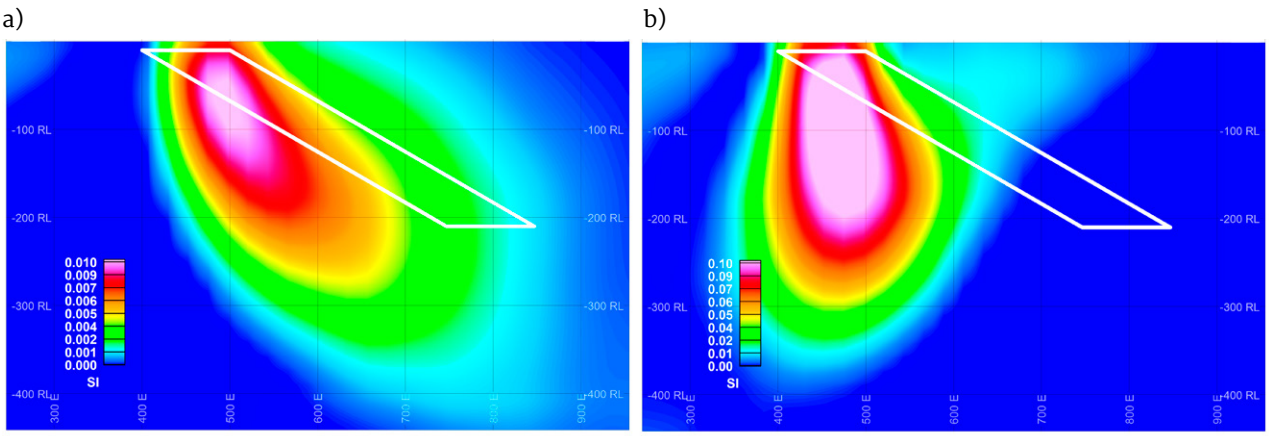

Fig. 17. Cross sections of inversion results of the synthetic model responses of Figure 16: a) the model with Q = 0 and b) the model with Q = 10. The original model body is outlined in white. Note the difference in the colour scales.

models demonstrated that the inversion algorithm manages to solve the general dip direction and depth extent for the model with Q = 0, although the inferred dip is too steep (Fig. 17a). However, for the model Q = 10 (Fig. 17b), the direction of the remanent magnetization greatly affects the solved dip direction as the recovered model body appears nearly vertical. The results provide an indication of the effects we may see in the Miihkali inversion results whenever black schists are present.

Inversion results

The magnetic inversion was performed for the entire study area (Figs. 3a–b).

Due to the strong remanent magnetization of the black schists, in particular, it is challenging to find reasonable ways to employ geological or petrophysical inversion constraints on the Miihkali region. Constraining the variation in the magnetic properties based on the density model would disregard the black schists altogether, as they may occur outside the density model bodies; similarly, guiding the inversion towards a reference model built from measured drill core susceptibilities would bias the calculation. Thus, the inversion was finally left unconstrained. The inversion parameters are presented in Table 1.

Looking at the recovered magnetic susceptibility model at various depths (Fig. 18), the shallow parts of the model reflect the known Miihkali massif rocks and black schists. The deeper parts of the magnetic structure, visible on the magnetic map (Fig. 18a) as long-wavelength anomalies, become clearly visible in the model at depths greater than 500 m below the surface.

The 3D model can be clipped to only show magnetic susceptibilities (k) exceeding a certain threshold value. In Figure 19a, clipping the model to show higher susceptibilities only (k > 0.05 SI), we can see a structure closely corresponding to the surface presentation of the Miihkali massif rocks, although the dip of the model structure can be considered unduly steep with regard to prior geological knowledge. With a lower threshold value (k > 0.025 SI) in Figure 19b, the deep-set curving "extensions" of the magnetic body (also detected in Fig. 18a) can be outlined.

Comparison of the recovered susceptibility model with drill-hole information (e.g. Fig. 20) draws attention to the dip and depth extent of high-susceptibility parts of the model. Considering the effects introduced in Figure 17, the remanent magnetization of the black schists (top part of drill hole JU-MI-81, bottom parts of the drill holes JU-MI-114 and JU-MI-78 in Figure 20) may well cause an overly vertical dip for the structure, as well as a false low-magnetization region on the eastern side of the black schists flanking the meta-ultramafic and gabbro rocks. In this case, it is difficult to estimate the exact effects of the remanent magnetization on the inversion results. In addition to the dip directions, the high total magnetization in the vicinity of the black schists (c. ten-fold in comparison to induced magnetization) may well cause the depth extent of the structures to be unreliably portrayed; comparison of the model and the measured susceptibilities certainly reveals inaccuracies in the inversion results. However, drill hole JU-MI-78 shows a section of high-susceptibility serpentinite rocks, and the inversion model susceptibilities also increase east of the drill hole; the top depth of the inversion structure fits the drilling results. This suggests that even though the recovered inversion model result is admittedly at least partially open to dispute, the model can still highlight interesting magnetic features outside the scope of the current drilling information.

Table 1. Parameters used in the magnetic 3D inversion.

Inversion parameter	Value
Mesh size	194 × 169 × 40 cells
Cell size	100 × 100 m, cell height increasing downwards
Sample interval	100 × 100 m
Maximum depth	4000 m
Data error	20 nT
Chifact	1.0
Model bounds	0.0–1.0 SI
Topography	Constant 150 m
Elevation	Constant 200 m
Depth weighting	β = 3.0, z_0 = 74.45
Initial and reference models	0.0 SI
Field parameters	B = 51219 nT, I = 74.5°, D = 7.5°

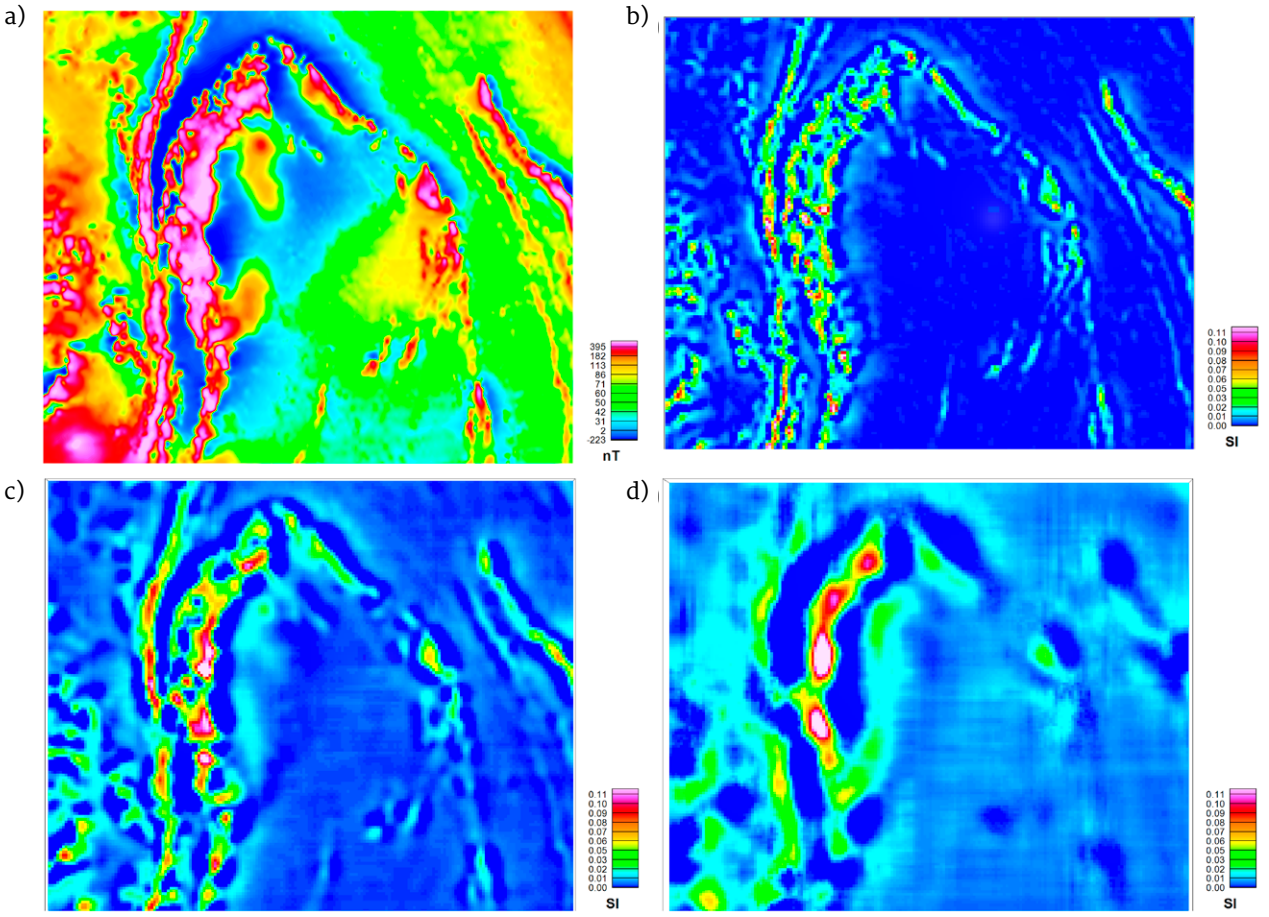

Fig. 18. Residual total magnetic intensity data (a) and the recovered magnetic susceptibility model at depths of b) 200 m, c) 500 m and d) 1000 m below the surface.

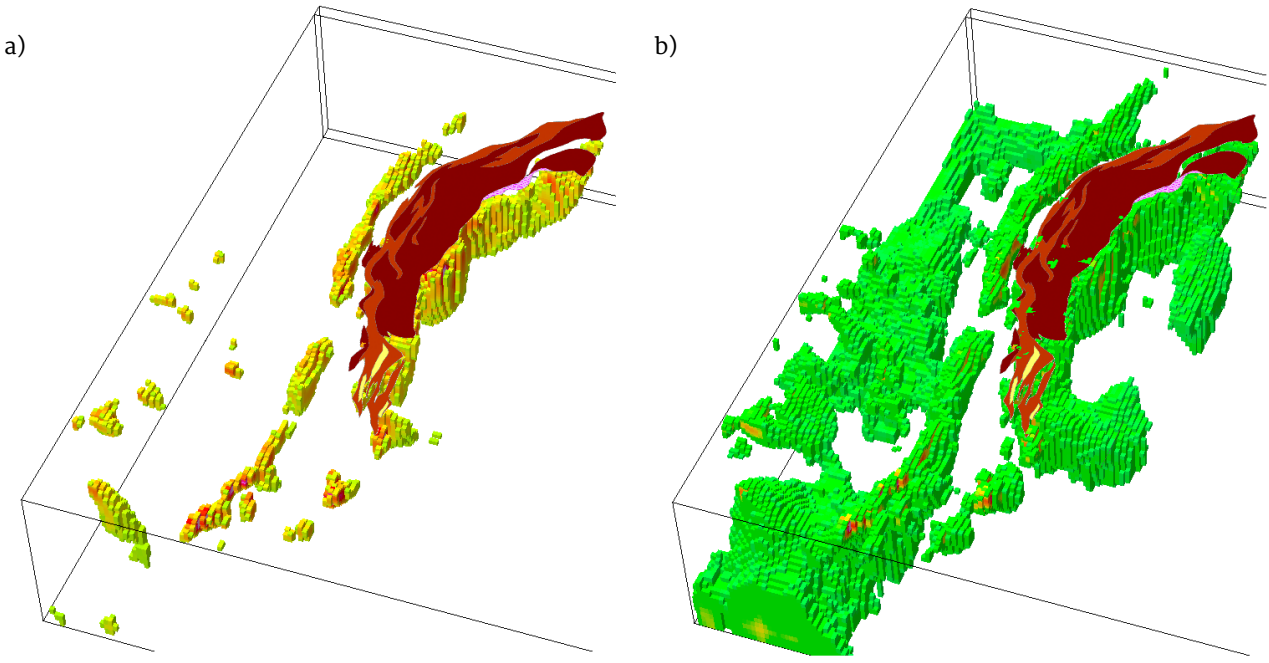

Fig. 19. Recovered magnetic susceptibility model clipped at a) 0.05 SI and b) 0.025 SI for the Miihkali massif, which is outlined in both a) and b) for its surface geology.

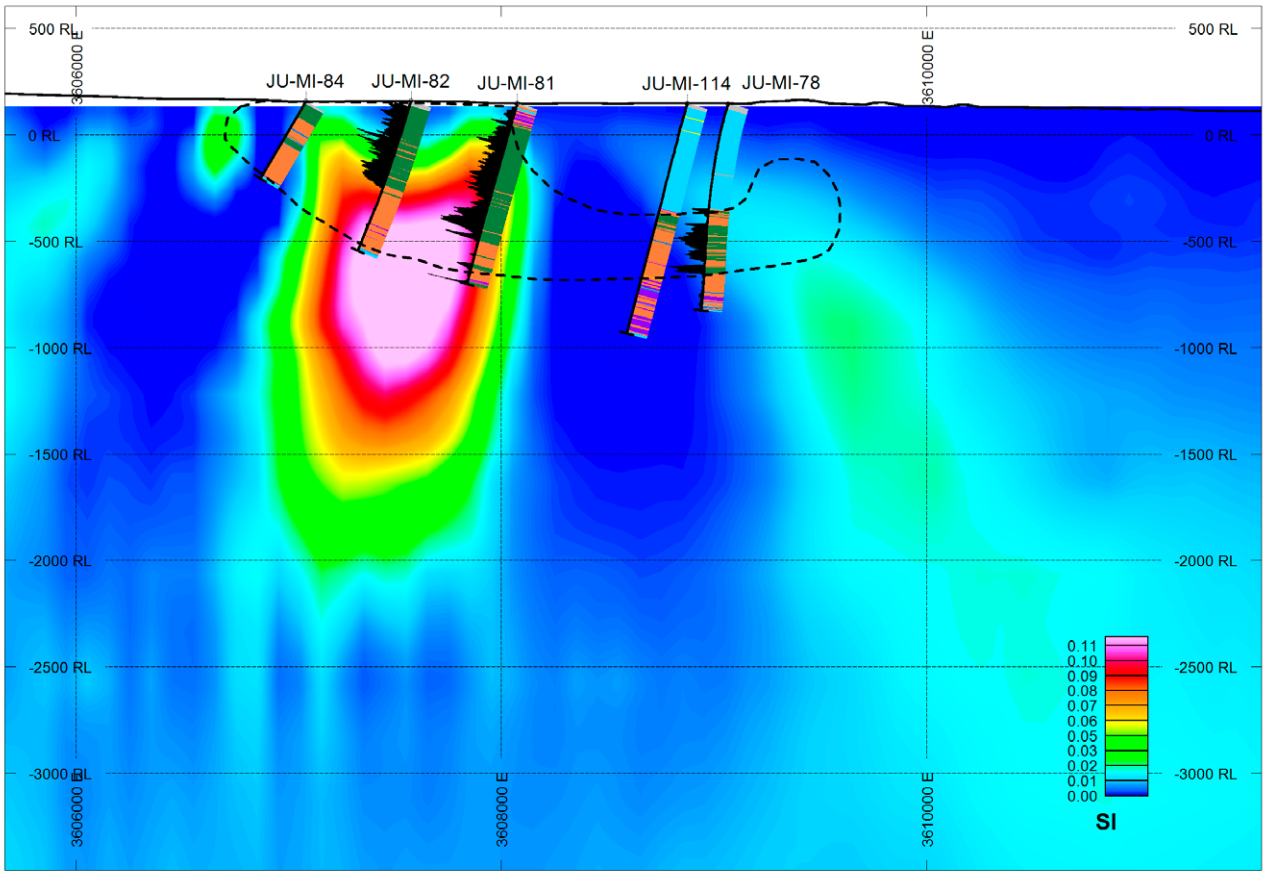

Fig. 20. Comparison of the recovered magnetic susceptibility model with drill-hole profile N=6989000. Magnetic susceptibilities logged from the drill holes are shown as black profiles plotted along the holes, and the anomalous density model is outlined with a dashed line. Drill-hole lithology colours: green = serpentinite, orange = OAUM rocks and metagabbros, purple = black schists, blue = mica schists.

DEEP ELECTROMAGNETIC SURVEYS

In the Outokumpu region, the Miihkali area is exceptionally favourable for electromagnetic (EM) measurements, as the area is located far from major sources of anthropogenic electromagnetic disturbances. This is particularly beneficial for ZTEM and AMT surveys, which utilize natural electromagnetic fields. Prior to the current project, scalar AMT (Soininen 1979, Lehtonen 1980) and Gefinex 400s (Kuronen et al. 2003) surveys had been carried out in the Miihkali area. New ZTEM and tensor AMT data were collected during this project. Figure 21 presents the survey lines of the aforementioned deep EM measurements plotted on airborne magnetic and electromagnetic maps. The airborne EM map (Fig. 21b) shows a shallow conductivity structure (generally < 50 m), which helps to assess the spatial correlation of surface and deep conductivity anomalies.

ZTEM survey

As a part of the Outokumpu mining camp project, GTK purchased a helicopter Z-axis tipper electromagnetic (ZTEM) survey that was carried out by Geotech Airborne Ltd in June 2013. The ZTEM system provides information from sources located in the depth range of approximately 0.5–2 km. Altogether, ~ 1250 line km were measured with line spacing of 500 m, 1 km and 2 km. Line spacing in the Miihkali area was either 1 or 2 km. The contractor provided 2D and 3D inversions of the ZTEM data (Geotech Ltd 2013). The description of the survey and the inversion results are presented in the same volume by Kurimo et al. (2016).

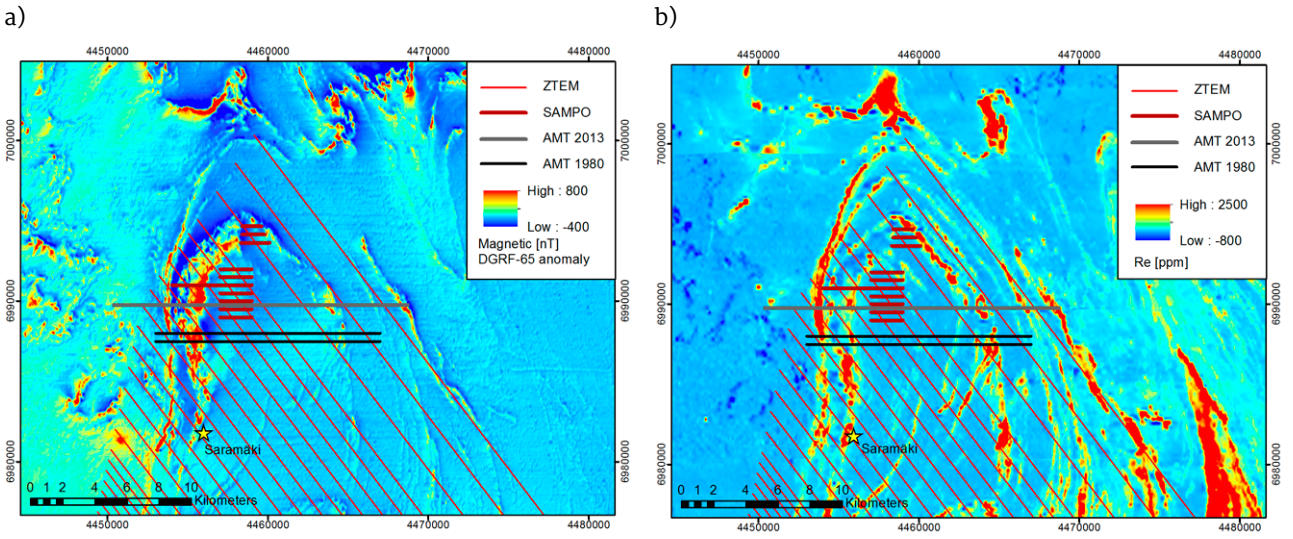

Fig. 21. Location of deep EM sounding profiles in the Miihkali area. The background image is a) an airborne magnetic and b) an airborne EM in-phase component map at 3222 Hz.

The ZTEM system measures naturally occurring magnetic field variations as the magnetotelluric (MT) technique (Condor Consulting Inc. 2012). From a geological point of view, the ZTEM system responds best to conductivity contrasts associated with large-scale geological features. The moving receiver measures the vertical magnetic field (H_z) and the horizontal components (H_x, H_y) are measured simultaneously at a base station. The processed data (tipper components) comprise the ratios of H_z/H_y and H_z/H_x, commonly referred to as the tipper ratios T_{zx} and T_{zy}. The data consist of 24 parameters in total: real (in-phase) and imaginary (quadrature) parts of the tipper transfer functions derived from the in-line (T_{zx}) and the cross-line (T_{zy}) components of six frequencies (25, 37, 75, 150, 300 and 600 Hz). It is noteworthy that H_z is generated by the horizontal conductivity contrasts (2D and 3D structures), and the system is consequently not sensitive to 1D (layered earth) structures. The obvious advantage of ZTEM is that multi-frequency deep EM data can be acquired from a large area in a short time.

It is well known that owing to the inherently ambiguous nature of geophysical data, significantly differing interpretations can be relevantly produced from the same data. However, features that are consistent between various interpretations are probably more reliable. Top views of 2D (interpolated) and 3D inversion results are compared in Figure 22. As an example of modelling differences, the Saramäki deposit area (Fig. 22a) is conductive in the 2D results, whereas 3D results do not show a clear conductivity anomaly associated with the target. On the other hand, the Saramäki area is not optimal for 2D inversion, as the conductivity anomalies are not perpendicular to the modelling lines (flight lines), which is a pre-assumption of 2D inversion. Therefore, the obtained conductivity structure could partly be a modelling artefact. Both results, however, show conductive graphite-bearing schist to the west of the deposit, which is clearly seen in the airborne EM results (Fig. 21b).

2D inversion is independently performed for each survey line, whereas 3D inversion uses all data simultaneously. Thus, for cases with a large line separation, 3D results may become unreliable, as the geoelectric structure is "under-sampled", that is, the penetration depth or the EM field is less than the line spacing. This might be the case in the NE part of the ZTEM survey area, where the line spacing was 2 km. The limitation of 2D inversion, in turn, is the abovementioned pre-assumption that the electrical structure is perpendicular to the modelled survey lines. This assumption is often likely to be violated in the study area. In this study, for example, in the north-easternmost part of the survey area, at least shallow conductors are elongated along the flight lines (e.g. see Fig. 21b). The other disadvantage of 2D inversion is that only 50% of ZTEM data are used, i.e. the in-line (T_{zx}, i.e. TE mode) component, as the TM mode tipper response is zero in a 2D model.

Figure 23 shows ZTEM models in a perspective view together with the surface geology. It can be seen from the images that both the 2D and 3D

a) b)

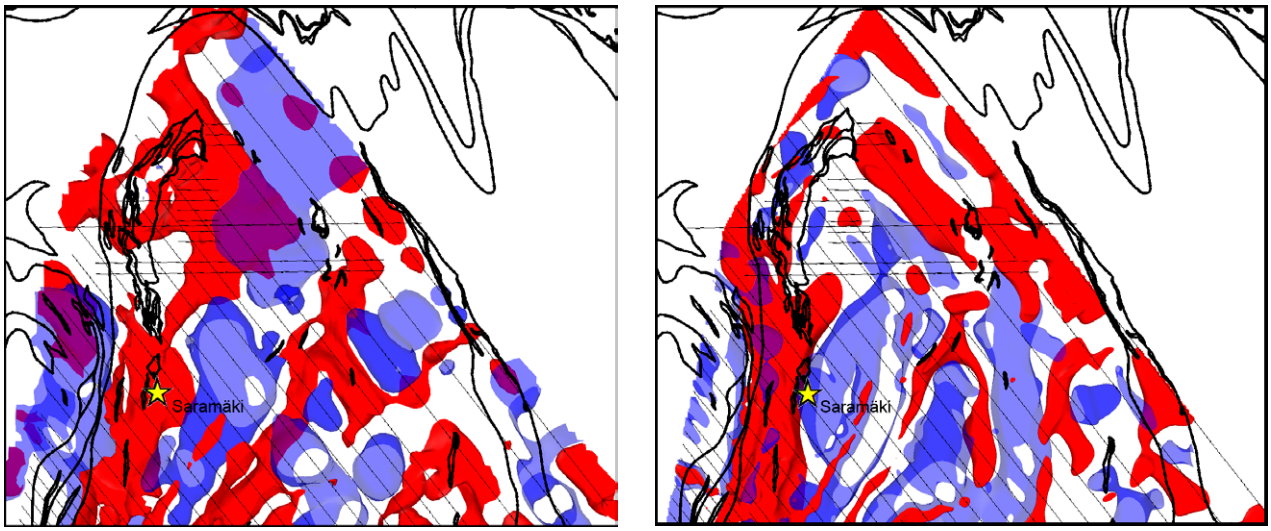

Fig. 22. Spatial distribution of ZTEM conductors: a) interpolated 2D and b) 3D inversion results. A red colour denotes 500 Ωm and blue (at 50% transparency) 3000 Ωm isosurfaces, respectively. The locations of the deep EM profiles presented in Figure 21 are shown as thin black lines. Thick black lines outline some main geological boundaries. The Saramäki deposit is indicated by a yellow star.

a) b)

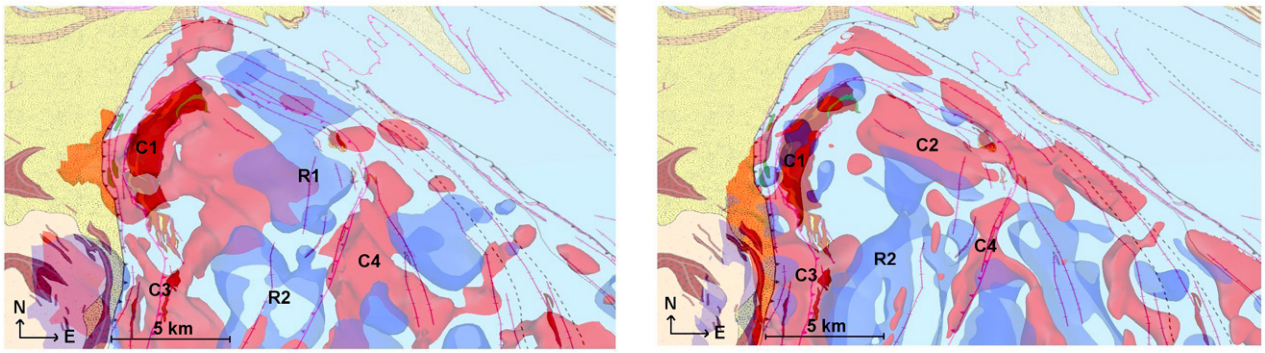

Fig. 23. Perspective views of a) the interpolated 2D and b) 3D ZTEM inversion results. A red colour denotes 500 Ωm and blue (50% transparency) 3000 Ωm isosurfaces, respectively. For reference, a transparent geological map is also presented. The view is from the south.

models show a pronounced conductor (C1), which appears spatially closely related to the Miihkali massif. The geological explanation for the apparently enhanced electrical conductivity of the serpentinite-metagabbro massif is unclear. It is noteworthy, however, that according to galvanic electrical conductivity measurements (Ketola 1973), for instance, Outokumpu serpentinities could themselves be quite conductive. The band of conductive sulphide-graphite bearing schists occurring along the western margin of the Miihkali mica gneiss area may also contribute to the observed ZTEM anomaly. Furthermore, the thin black schist layers and/or sulphides frequently occurring in or at the serpentinite body margins certainly cause EM anomalies. In the 2D model images, the C1 conductor is seen to gently dip eastwards below an overlying resistive unit (R1). In the 3D model, a deep conductor C2 is detected at the depths of 500–750 m. Although the deep conductor C2 is absent in 2D inversion results, many conductive and resistive features are quite similar (C1, C3, C4 and R2) in both the 2D and 2D inversion results. The conductor C2 is located in the area of widely spaced survey lines (2 km), and its existence should thus be tested with drilling or by additional deep EM measurements.

AMT soundings

AMT soundings were performed in the Miihkali area in 1979–1980 and during the current project. The older measurements were performed by Outokumpu Oy with scalar AMT equipment (Soininen 1979, Lehtonen 1980). In addition, Lakanen (1981) reported results from control source AMT tests in Miihkali. In the scalar measurement of the 1979–1980 survey, a single polarization impedance sounding curve was acquired and the sensors needed to be rotated in order to obtain information from other polarizations. The system measured nine apparent resistivity values in the frequency range of 8–3700 Hz. The older survey was carried out along a 14 km long profile, which transected the Miihkali mica gneiss area in the E–W direction (Fig. 21). The measurements in "TE mode" were performed using 200 m site spacing and in "TM mode" at 400 m site spacing. In the TE mode, the induction coil magnetometer is perpendicular and electric dipole parallel to the geoelectric strike direction. In the TM mode, the electric dipole is perpendicular and induction coil magnetometers parallel to the strike. Therefore, when using these concepts, the structure is assumed to be 2D, and in the case of Miihkali the 2D electrical conductivity structure was assumed to be N–S elongated. One-dimensional interpretation was carried out for both modes and results were displayed as pseudosections. An eastwards-dipping conductor was interpreted to follow the lower boundary of the Miihkali mica gneiss/Sukkulansalo nappe. The results also inferred a shallower depth for the central part of the mica gneiss unit (depths 600–900 m) followed by an abrupt increase in depth to the east. In the easternmost part, the unit was interpreted to be thinning eastwards.

GTK has recently carried out tensor AMT surveys using acquisition procedures that include remote referenced measurements (Gamble et al. 1979), robust processing (Egbert & Booker 1986, Chave et al. 1987) and subsequent 1D/2D/3D modelling and inversion. The instruments used and the surveys have been described in Lahti (2015). In the measurement procedure, five components (H_x, H_y, H_z, E_x and E_y) of the EM field are simultaneously recorded. In addition, a remote reference site records two components (H_x and H_y) during the survey, which helps to reduce uncorrelated EM disturbances. During this project, AMT data were acquired along five profiles, including one for the Miihkali area. The AMT data at the frequency range 1–10 000 Hz were acquired during the day, whereas long night recordings enabled data to be obtained in the frequency range of 0.01–10 000 Hz. Measurements were performed using two Metronix 24bit ADU-07e broadband electromagnetic acquisition systems. Robust remote reference processing mostly yielded good data quality, particularly for data recorded during the night.

The central part of the Miihkali mica gneiss unit is appropriate for E–W 2D modelling, as it is characterized by roughly N–S elongated, laterally extensive conductors indicated by low-altitude airborne electromagnetic data. The remote referenced AMT data were acquired at 21 sites along an 18 km long E–W profile. The profile is located ca. 2 km to the north of the old Outokumpu Oy AMT profile. 2D inversion was jointly carried out for the TE and TM data using the nonlinear conjugate gradient algorithm by Rodi and Mackie (2001). It is well known that galvanic distortion can shift apparent resistivity curves (e.g. Wannamaker et al. 1984, Jiracek 1990). Therefore, an error floor of 15% was assigned for the apparent resistivity and 5% for the phase, respectively. Satisfactory fit and stable inversion solution was obtained for the profile with the RMS error of 3.3. The inversion result (Fig. 24a) shows a gently eastwards dipping conductor in the Miihkali mica gneiss located at the bottom of the inferred Miihkali nappe, reaching depths greater than 1 km at approximately the eastern margin of the oval Miihkali nappe. Further to the east, the conducting feature vanishes. The conductivity model is mainly consistent with the old AMT survey results and the new ZTEM 2D model (Fig. 24b). The gently dipping conductor is probably related to N–S elongated airborne EM anomalies that are seen to coincide with the Miihkali serpentinite massif and black schist band along the western margin of the allochthonous Miihkali mica gneisses. The old AMT results inferred a steeply west-dipping conductor at the eastern margin of the Miihkali nappe, which is probably related to conductor C4 seen in ZTEM results. The AMT model in Figure 24 does not clearly show this feature, most likely because the profile is located north of C4 and the old AMT profile. The ZTEM conductor C2 in 3D ZTEM inversion results is not seen in the new AMT 2D model.

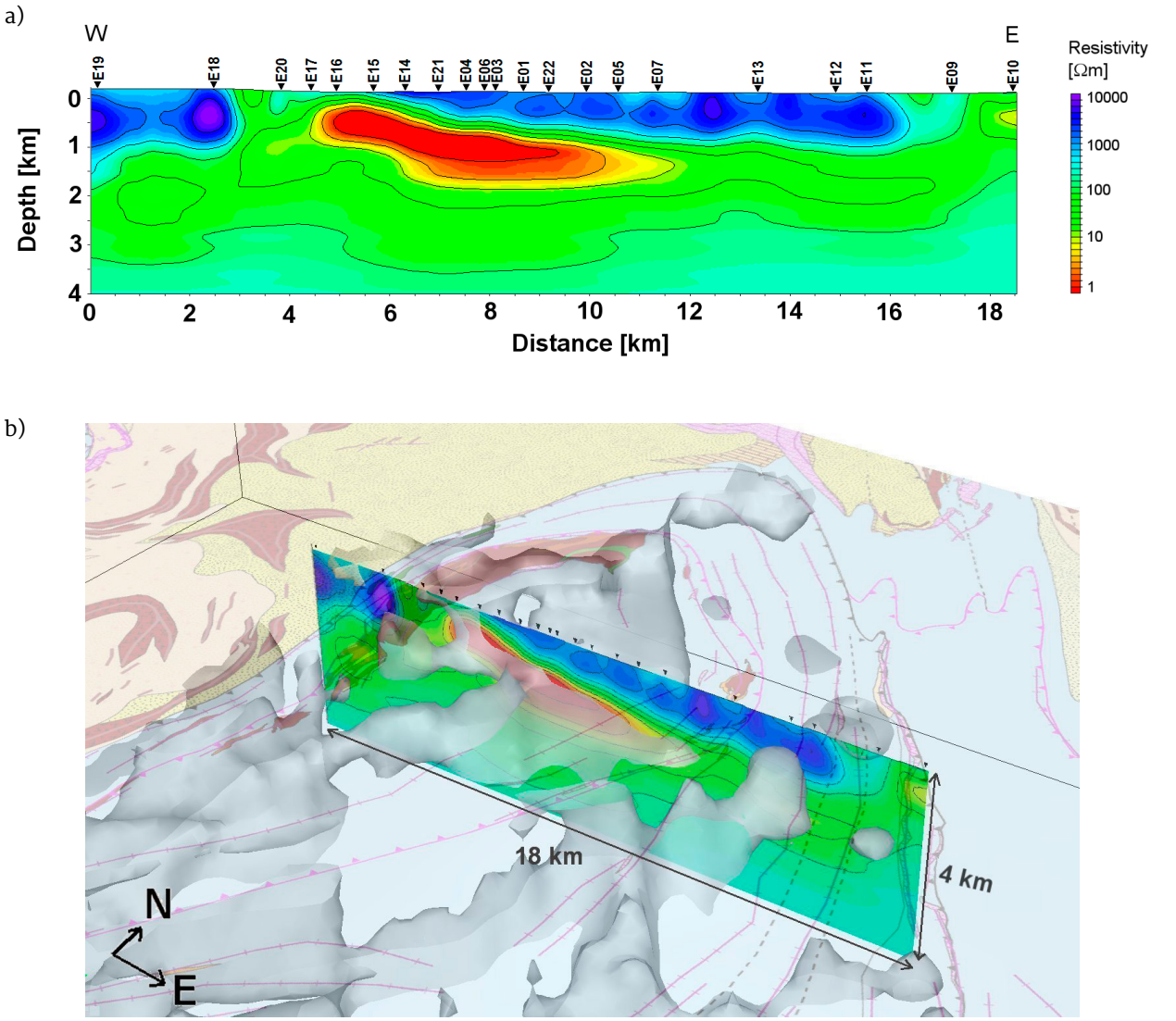

Fig. 24. a) New AMT 2D inversion model (RMS = 3.3) and b) comparison of new AMT 2D and interpolated ZTEM 2D models (grey 500 Ωm isosurface). For reference, surface geology is also shown as a transparent layer. The view is from the southeast.

Sampo soundings

Sampo (Gefinex 400S) is a frequency domain EM system developed by the Outokumpu Oy for Outokumpu Exploration and GTK (Aittoniemi et al. 1987, Soininen & Jokinen 1991, Sipola 2002). The practical maximum survey depth of the method is less than 1 km, but if dense measurement spacing is used, the spatial resolution is higher compared to other deep EM techniques. The measurements in the Miihkali area were carried out in 2002 during the joint Outokumpu-GTK GEOMEX project (Kuronen et al. 2003) in two target areas at Kiskonjoki and Lipaspuro. The measurements were performed using a "broadside" loop configuration in which the transmitter and receiver were located at opposite sides of the E–W directed profiles. The distance between the transmitter and receiver was 500 m. The line spacing was 500 m and the station spacing 100 m. Altogether 224 soundings were made along 10 profiles with a total length of 21.4 km. The acquired data were interpreted using 1D inversion software developed by GTK and the results were visualized as pseudosections (Fig. 25).

The densely spaced Sampo soundings enable distinguishing separate conductors in the Miihkali serpentinite massif and within the western margin of the Miihkali mica gneiss. These conductors are probably all superimposed in one larger coherent feature in the image of the 2D AMT results due to the larger site distance and the smooth 2D inversion procedure used (Fig. 25). The Sampo method

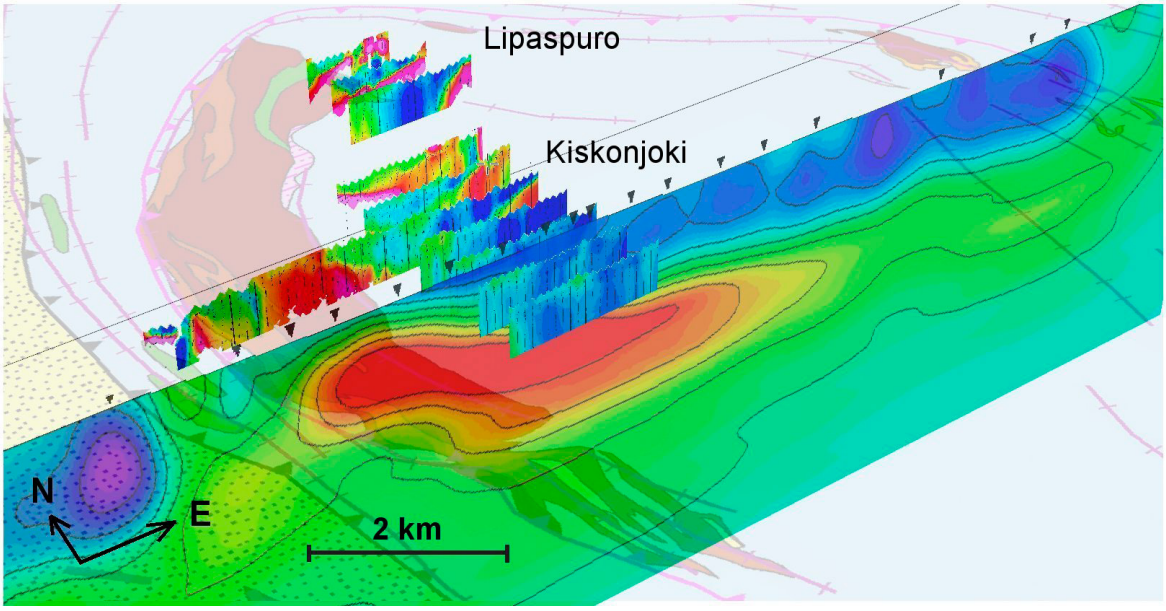

Fig. 25. A stacked image of the Lipaspuro and Kiskonjoki Sampo (Gefinex 400S) 1D conductivity model pseudo-sections. An image of the AMT 2D model and the surface geology, the latter as a transparent map layer, are also presented. Orange to red colours denote conductive features. The view is from the southwest.

detected conductors in the Lipaspuro area and in the northernmost profiles of the Kiskonjoki survey area (Kuronen et al. 2003). To the south, no significant shallow conductors were detected, which is in agreement with all the deep EM results previously presented here.

A total of four drill holes (1382.85m) were drilled during 2001–2002 at the Kiskonjoki prospect. A significant intersection of Outokumpu-type rocks was made, starting approximately at the depth of 300 m. The drill hole is located at the northernmost Sampo survey profiles at Kiskojoki. The drilled Outokumpu rocks are seen as conductors in the Sampo models.

The nearly flat-lying conductor at Lipaspuro most likely represents black schist on the top of an Outokumpu-type formation or within mica schist (Kuronen et al. 2002). The GEOMEX project had no drilling resources to test these Sampo results further.

Electrical conductivity of Miihkali drill core samples

Petrophysical measurements of the Miihkali drill core samples indicate significant resistivity variations in the target area. This is illustrated by Figure 26, showing galvanic resistivity loggings for four drill holes. The resistivity of the granitic gneisses, mica gneisses and schists is high, mainly above 10^5 Ωm (JU-MI-80). The resistivity of the skarns, carbonate rocks and metabasites is typically over 10^4 Ωm (JU-MI-81, JU-MI-85). Resistivities of the Miihkali serpentinites are lower, usually 10^1 – 10^4 Ωm (JU-MI-81, JU-MI-85). The serpentinites therefore have a resistivity contrast of about 2–4 orders of magnitude with background rocks, which together with narrow and extremely conductive black schists layers (<10^1 Ωm) could at least partly explain the deep EM anomalies of the area.

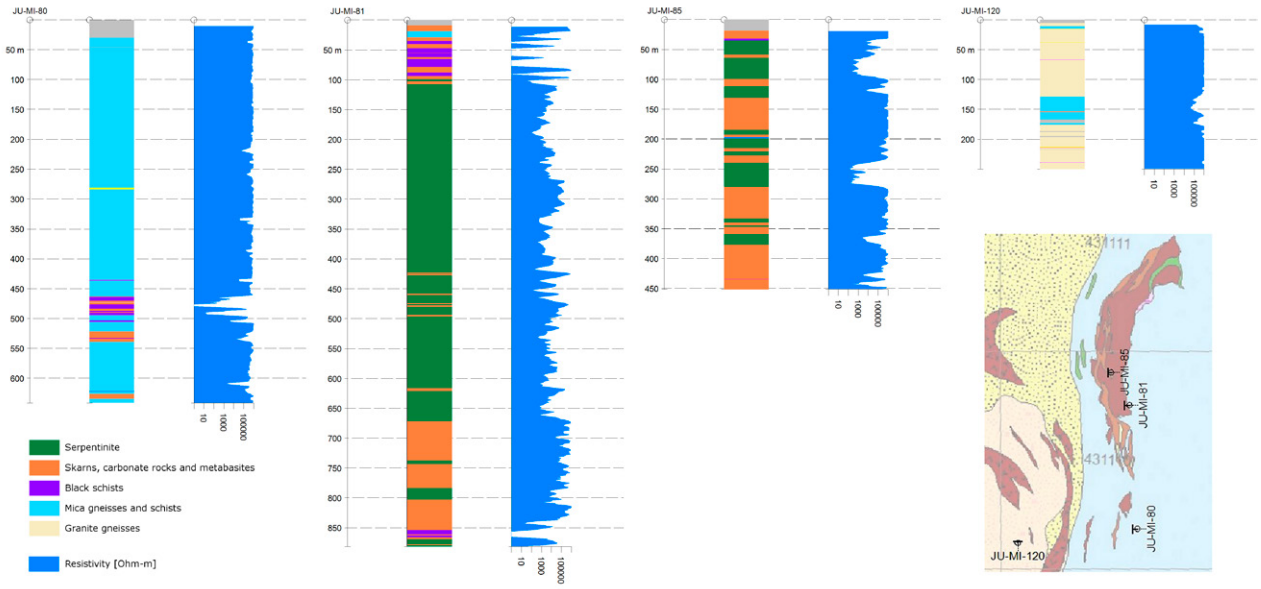

Fig. 26. Lithology and resistivity logs of four Miihkali area drill cores with a map showing the location of the drill holes.

CONCLUSIONS

In this research, both forward modelling and inversion approaches were employed in potential field data modelling. The forward modelling of the residual gravity data benefited from the relatively dense drilling in the region, as the model could be constrained with the drill core logging results and the related density values. In general, the regional model and the residual model are both well in accordance with the geological cross-sections and drilling results, which implies that the current drilling scope covers the majority of the gravity sources. However, some (relatively small) discrepancies remain between the density model and the drill core logs, mainly because of inconsistencies and inordinate generalization in the rock identification and naming in the existing drill core logging data, resulting in possibly biased density classifications and density model / drill core log comparisons.

High remanent magnetization intensities pose a challenge in magnetic modelling and inversion. The direction of remanent magnetization differs notably from the inducing field direction, and as such the high Q ratios in the region should not be ignored in modelling. However, accommodating magnetic inversion techniques to include remanent magnetization over large areas is still largely an unfeasible task. In Miihkali, most notably the black schists with high Q values contort the inversion results and render the inversion model results at least locally imprecise; however, in limited regions, the inversion model was related to the drill-core data and could be used as guidance, as long as the inaccuracies due to the high remanent magnetization intensities are taken into account.

In general, the potential field models do not reveal entirely new and unknown features in the Miihkali region. The deep-set magnetic and high-density features running along the main Miihkali massif have not, based on the potential field models, been thoroughly covered by drilling, and further research on these features could provide some new information on the Miihkali massif and its geological setting.

Deep EM results demonstrate conductors related to the western margin of the Miihkali mica gneisses and the Miihkali serpentinite massif. The ZTEM and AMT 2D inversion results show a gently eastwards-dipping conductor in the Miihkali mica gneiss located at the bottom of the inferred Miihkali nappe, reaching depths greater than 1 km at approximately the eastern margin. The gently dipping conductor is probably related to N–S elongated airborne EM anomalies that are seen to coincide with the Miihkali serpentinite massif and black schist band along the western margin of the allochthonous Miihkali mica gneisses. In most cases, the surficial EM anomalies indicated by

low-altitude airborne surveys can be connected to deep ZTEM anomalies, showing the continuation of elongated conductive features to greater depths. The densely spaced Sampo soundings distinguish separate conductors in the Miihkali serpentinite massif and within the western margin of the Miihkali mica gneisses. In addition, the Sampo technique detected conductors in the Kiskonjoki prospect, which proved to be caused by Outokumpu-type rocks intersected by drillings at the depth of 300 m.

ACKNOWLEDGEMENTS

The authors acknowledge reviews of the manuscript by Aimo Hattula and Markku Pirttijärvi.

REFERENCES

Ahokas, T. 1980. Petrofysikaalisia sovellusesimerkkejä. In: Pesonen, L. J. (ed.) Sovelletun geofysiikan jatkokurssi 1979–1980 6.33.35. Teknillinen korkeakoulu. (in Finnish)

Aittoniemi, K., Rajala, J., & Sarvas, J. 1987. Interactive Inversion Algorithm and Apparent Resistivity Versus Depth (ARD) Plot in Multifrequency Depth Soundings. Acta Polytechnica Scandinavica Applied Physics Series 157. 34 p.

Bedrock of Finland – DigiKP. Digital map database [Electronic resource]. Espoo: Geological Survey of Finland [referred 14.04.2016]. Version 2.0.

Chave, A. D., Thomson D. J. & Ander, M. E. 1987. On the robust estimation of power spectra, coherences and transfer functions. Journal of Geophysical Research 92, 633–648.

Condor Consulting Inc, 2012. THE ZTEM PRIMER. Rev 3.

Egbert G. D. & Booker J. R. 1986. Robust estimation of geomagnetic transfer functions. Geophysical Journal of the Royal Astronomical Society 87, 173–194.

Gamble, T., Goubau, W. & Clarke, J. 1979. Magnetotellurics with a remote magnetic reference. Geophysics 44, 53–68.

Geotech Ltd. 2013. Report on a helicopter-borne Z-axis tipper electromagnetic (ZTEM) and aeromagnetic geophysical survey, Outokumpu Mining Camp Area, Finland. Project AB130076.

Gaál, G. & Parkkinen, J. 1993. Early Proterozoic ophiolite-hosted copper-zinc-cobalt deposits of the Outokumpu type. In: Kirkham R.V., Sinclair, W.D., Thorpe, R.I. & Duke, J.M. (eds) Mineral Deposit Modeling. Geological Association of Canada, Special Paper 40, 335-341.

Gaál, G., Koistinen, T. & Mattila, E. 1975. Tectonics and stratigraphy of the vicinity of Outokumpu, North Karelia, Finland : including a structural analysis of the Outokumpu ore deposit. Geological Survey of Finland, Bulletin 271. 67 p.

Hallikainen O. 1980. Kaivospiirihakemus Polvijärvi, Saramäki, kaiv.rek.nro 2501/1a. Outokumpu Oy. (in Finnish)

Hautaniemi, H., Kurimo, M., Multala, J., Leväniemi, H. & Vironmäki, J. 2005. The "Three In One" aerogeophysical concept of GTK in 2004. In: Airo, M.-L. (ed.) Aerogeophysics in Finland 1972-2004: Methods, System Characteristics and Applications. Geological Survey of Finland, Special Paper 38, 21–74.

Jiracek, G. 1990. Near surface and topographic distortions in electromagnetic induction, Surv. Geophys., 11, 163–203.

Ketola, M. 1973. Outokummun alueen geofysiikasta. Outokumpu Oy, unpublished report. 15 p. (in Finnish)

Ketola, M. 1974. Karttalehdellä 4313 suoritetun alueellisen gravimetraustuloksen tulkinta profiililla X=990,00. Outokumpu Oy, unpublished report. 1 p. (in Finnish)

Koistinen, T. 1981. Structural evolution of an early Proterozoic strata-bound Cu-Co-Zn deposit, Outokumpu, Finland: Transactions of the Royal Society of Edinburgh: Earth Sciences, 72, 115–158.

Kontinen, A. 1998. The nature of the serpentinites, associated dolomite-skarn-quartz rocks and massive Co-Cu-Zn sulphide ores in the Outokumpu area, eastern Finland. In: Hanski, E. & Vuollo, J. (eds) International ophiolite symposium and field excursion: generation and emplacement of ophiolites through time, August 10–15, 1998, Oulu, Finland. Abstracts, excursion guide. Geological Survey of Finland, Special Paper 26, p. 33.

Kontinen, A., Peltonen, P. & Huhma, H. 2006. Description and genetic modelling of the Outokumpu-type rock assemblage and associated sulphide deposits. Final technical report for GEOMEX J.V., Workpackage Geology. Geological Survey of Finland, archive report M10.4/2006/1. 378 p.

Kurimo, M., Lahti, I. & Nousiainen, M. 2016. ZTEM survey in the Outokumpu region. In: Aatos, S. (ed.) Developing Mining Camp Exploration Concepts and Technologies – Brownfield Exploration Project 2013–2016. Geological Survey of Finland, Special Paper 59. (this volume)

Kuronen, U., Kontinen, A. & Kokkonen, J. 2003. GEOMEX project report. (unpublished report)

Lahti, I. 2015. Audiomagnetotelluric (AMT) measurements: A new tool for mineral exploration and upper crustal research at the Geological Survey of Finland. In: Sarala, P. (ed.) Novel Technologies for greenfield exploration. Geological Survey of Finland, Special Paper 57, 155–172.

Lakanen, E. 1981. Lähetin AMT (LAMT) kokeilu Miihkalissa ja Saramäessä 1980. Outokumpu Oy:n malminetsinnän raportit. (in Finnish)

Lehtonen, T. 1980. AMT-mittaus Miihkalin Kaaren yli. Outokumpu Oy:n malmin-etsinnän raportit. (in Finnish)

Lehtonen, T. 1981. Outokummun alueen kivilajien petrofysikaalisista ominaisuuksista. Unpublished master's thesis, Helsinki University of Technology. 77 p. (in Finnish)

Leväniemi, H. 2016. Petrophysical parameters and potential field modelling in the Outokumpu Belt. In: Aatos, S. (ed.) Developing Mining Camp Exploration

Concepts and Technologies – Brownfield Exploration Project 2013–2016. Geological Survey of Finland, Special Paper 59. (this volume)

Li, Y. & Oldenburg, D. W. 1996. 3-D inversion of magnetic data. Geophysics 61 (2), 394-408.

Li, Y. & Oldenburg, D. W. 1998. 3D inversion of gravity data. Geophysics 63, 109–119.

Park, A. F. 1988. Nature of the early Proterozoic Outokumpu assemblage, eastern Finland. Precambrian Research 38, 131-146.

Park, A. F. & Bowes, D. R. 1983. Basement-cover relationships during polyphase deformation in the Svecokarelides of the Kaavi district, eastern Finland. Transactions of the Royal Society of Edinburgh: Earth Sciences 74, 95-118.

Park, A. F. & Doody, J. J. 1990. Structural styles in the deep levels of an Early Proterozoic foreland thrust belt. In: Lewry, J. F. & Stauffer, M. R. (eds) The Early Proterozoic Trans-Hudson Orogen of North America. Geological Association of Canada, Special Paper 37, 465-482.

Park, A. F., Bowes, D. R., Halden, N. M. & Koistinen, T. J. 1984. Tectonic evolution at an early Proterozoic continental margin: the Svecokarelides of eastern Finland. Journal of Geodynamics 1, 359-386.

Peltonen, P., Kontinen, A., Huhma, H. & Kuronen, U. 2008. Outokumpu revisited: New mineral deposit model for the mantle peridotite-associated Cu-Co-Zn-Ni-Ag-Au sulphide deposits. Ore Geology Reviews 33, 559-617.

Rodi, W. & Mackie, R. 2001. Nonlinear conjugate gradients algorithm for 2-D magnetotelluric inversion. Geophysics 66, 174-187.

Saastamoinen, J. 1972. Miihkalin jakson tutkimukset v. 1966-72. Outokumpu Oy:n malminetsinnän raportit 001/4311, 4313/JYS/72. (in Finnish)

Säntti, J., Kontinen, A., Sorjonen-Ward, P., Johanson, B. & Pakkanen, L. 2006. Metamorphism and chromite in serpentinized and carbonate-silica–altered peridotites of the Paleoproterozoic Outokumpu-Jormua ophiolite belt, eastern Finland. International Geology Review 48, 494–546.

Sipola, V.-P. 2002. A new data processing and interpretation program for the Sampo electromagnetic multifrequency sounding system. Master's thesis, Helsinki University of Technology, Otaniemi, 69 p. (in Finnish with an English abstract)

Soininen, H. 1979. AMT-luotaus Miihkalin ns. Pitkällä profiililla. Outokumpu Oy:n malminetsinnän raportit. (in Finnish)

Soininen, H. & Jokinen, T. 1991. Sampo, a new wide-band electromagnetic system. European Association of Exploration Geophysics 53rd meeting and Technical Exhibition, Florence, Italy. Technical programme and Abstracts of papers, 366–367.

Sorjonen-Ward, P., Nironen, M. & Luukkonen, E. 1997. Greenstone associations in Finland. In: De Wit, M. J. & Ashwal, L. (eds) Greenstone belts. Oxford Monographs on Geology and Geophysics 35, 677–698.

Väyrynen, H. 1939. On the geology and tectonics of the Outokumpu ore field and region. Bulletin de la Commission Géologique Finlande 124, 1–91.

Wannamaker, P., Hohmann, G. W. & Ward, S. 1984. Magnetotelluric responses of three-dimensional bodies in layered earths, Geophysics, 49, 1517–1533.

Wegmann, C. E. 1928. Über die tectonik der jüngeren Faltungen in Ostfinnland. Fennia 50, 1–22.

Wegmann, C. E. 1929. Beispiele tektonischer Analysen des Grundgebirges in Finnland. Bulletin de la Commission Géologique de Finlande 87, 98-127.